Interlaminar Shear Performance of High Temperature Composites

THESIS

Wallis, Tyler A., Capt, USAF
AFIT-ENY-MS-19-M-250

DEPARTMENT OF THE AIR FORCE
AIR UNIVERSITY

AIR FORCE INSTITUTE OF TECHNOLOGY

Wright-Patterson Air Force Base, Ohio

DISTRIBUTION STATEMENT A
APPROVED FOR PUBLIC RELEASE; DISTRIBUTION UNLIMITED.

The views expressed in this document are those of the author and do not reflect the official policy or position of the United States Air Force, the United States Department of Defense or the United States Government. This material is declared a work of the U.S. Government and is not subject to copyright protection in the United States.

AFIT-ENY-MS-19-M-250

INTERLAMINAR SHEAR PERFORMANCE OF HIGH TEMPERATURE COMPOSITES

THESIS

Presented to the Faculty
Department of Aeronautics and Astronautics
Graduate School of Engineering and Management
Air Force Institute of Technology
Air University
Air Education and Training Command
in Partial Fulfillment of the Requirements for the
Degree of Master of Science in Materials Science

Wallis, Tyler A., BS
Capt, USAF

March 2019

DISTRIBUTION STATEMENT A
APPROVED FOR PUBLIC RELEASE; DISTRIBUTION UNLIMITED.

AFIT-ENY-MS-19-M-250

INTERLAMINAR SHEAR PERFORMANCE OF HIGH TEMPERATURE COMPOSITES

THESIS

Wallis, Tyler A., BS
Capt, USAF

Committee Membership:

Marina B. Ruggles-Wrenn, PhD
Chair

Thomas G. Eason, PhD
Member

Eric L. Jones, PhD
Member

AFIT-ENY-MS-19-M-250

Abstract

Interlaminar shear properties of a high temperature polymer matrix composite (HTPMC) and a ceramic matrix composite (CMC) were evaluated at elevated temperature. Two variants of the HTPMC were studied. Both consisted of a high-temperature polyimide (AFR-PE-4) matrix reinforced with Astroquartz-III pre-impregnated glass fabric woven in an eight-harness-satin weave. The first HTPMC variant also contained stainless steel foil at the midplane, while the second HTPMC variant did not. The interlaminar shear strength (ILSS) of both variants of the HTPMC was evaluated at 204°C in laboratory air. The addition of the stainless steel foil resulted in significant loss of ILSS for the HTPMC. The CMC studied in this work was fabricated via chemical vapor infiltration. The CMC had an oxidation-inhibited matrix consisting of alternating layers of SiC and B_4C and was reinforced with Hi-Nicalon^{TM}fibers woven in a five-harness-satin weave. Fiber preforms had pyrolytic carbon coating and boron carbide overlay applied. The ILSS of the CMC was measured at 1300°C in laboratory air. Additionally, creep performance in interlaminar shear of the CMC was evaluated at 1300°C in air and in steam. The creep behavior was assessed for interlaminar shear stresses varying from 12 MPa to 20 MPa in air and in steam. In air and in steam, creep run-out of 100 h was achieved at 13 MPa. Both primary and secondary creep regimes were noted in all tests. Presence of steam had little effect on creep performance. The retained properties of the specimens that attained run-out were characterized. Pre- and post-test composite microstructures were examined to evaluate damage and failure mechanisms.

Acknowledgements

First, I would like to thank God for this opportunity and seeing me through this last 18 months. I would like to thank my advisor, Dr. Ruggles-Wrenn, for her unrelenting support and guidance throughout my entire time at AFIT. Her willingness to spend however much time was necessary for me to understand course material or research questions was invaluable and inspiring.

I would also like to thank Jamie Smith and Mike Ranft for assisting me whenever I needed help at a moment's notice. In addition, I would like to thank Brian Crabtree and everyone else at the machine shop who always turned around my short suspense requests with no issues or complaints. I am also thankful for Major Ryan Kemnitz for spending hours with me on the SEM.

To my classmates, the ENY faculty, and the AFIT support staff: thank you for ensuring that I found all of the answers to my questions and that graduated in one piece.

Finally, I want to thank my wife for her endless support and understanding while I spent long nights and weekends in front of school work. Without her love and encouragement, earning this degree would not have been possible.

Wallis, Tyler A.

Table of Contents

List of Figures

Figure Page

Figure Page

Figure Page

List of Tables

INTERLAMINAR SHEAR PERFORMANCE OF HIGH TEMPERATURE COMPOSITES

I. Introduction

1.1 Motivation

In an age where materials are continually being pushed to their thermal and structural limits, more resilient materials are required to meet these growing design demands. While strength and heat resistance enhancement are primary concerns for designers, weight savings is just as critical in the applications where these materials are utilized. Generally, one way to bolster thermal and strength characteristics is to increase the amount of structural material or use a material with higher density. Both of these methods increase the overall weight of the structure. Due to the unique properties of composites, thermal resistance and strength can be increased with a relatively low density material when compared to conventional materials. Composite materials offer several advantages when compared to conventional monolithic materials such as steel and aluminum as illustrated in Figure 1. Composite materials excel in multiple design arenas and the continuous evolution of materials and processing used to manufacture composites increase their capabilities.

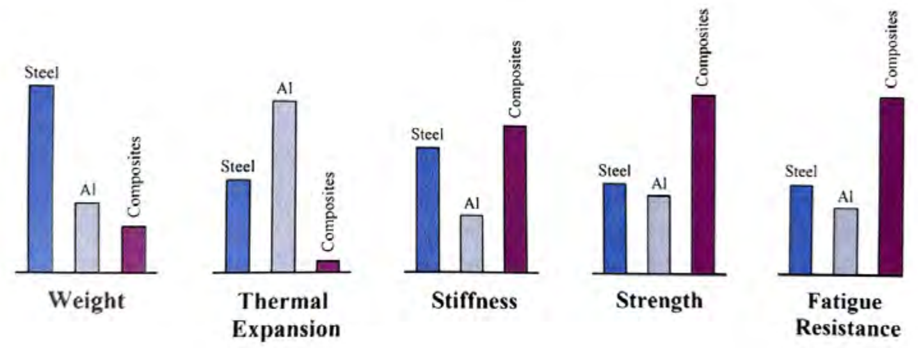

Figure 1. Comparison of conventional monolithic materials and composite materials. Figure from [1]

Depending on design requirements and operating environments, different classifications of composites are available (see Figure 2).

	MATRIX			
REINFORCEMENT	Polymer	Metal	Ceramic	Carbon
Polymer	X	X	X	X
Metal	X	X	X	X
Ceramic	X	X	X	X
Carbon	X		X	X

Figure 2. Types of Composites. Figure from [2]

These different classes are composed of polymer matrix composites (PMCs), ceramic matrix composites (CMCs), metal matrix composites (MMCs), and carbon-carbon composites (CCCs). Different combinations of fibers and matrix materials have many advantages or disadvantages depending on the structural requirements and operating environments. PMCs and CMCs will be the focus of this research.

PMCs are used on many structural applications because of their high strength to weight ratios, excellent corrosion, and fatigue resistance. PMCs are much simpler to manufacture than MMCs and CMCs due to the low processing temperatures required to produce a PMC[3]. They do however have some undesirable attributes such as low bearing and shear strength, as well as relatively low temperature resistance. As the structural requirements for composites continue to grow, solutions to address these weaknesses are the focus of several research efforts.

CMCs combine the formidable strength and heat resistant properties of ceramics while minimizing the poor fracture toughness characteristics. Continuous improvements in processing, as well as advancements in matrix design, have allowed CMCs to operate in unprecedented environments while maintaining structural integrity. Tuning the interface between the fibers and matrix while allowing cracks to deflect around the fibers can help increase fracture toughness.

1.2 Problem Statement

New technology and processing techniques allow the use of composites as high strength, low weight alternatives in aggressive environments that were historically reserved for special alloys. The mechanical properties of these new composites must be evaluated in simulated environments to determine the viability of these materials. While combining two or more dissimilar materials at room temperature may produce known and stable conditions, the same may not be true in different environments. While it is important to understand the baseline characteristics of a new composite in a mild environment (room temperature/normal humidity/etc.), the composite must be tested in aggressive environments to determine its ultimate limits. Additionally, new techniques for manufacturing composites require baseline testing and rigorous vetting of the extreme limits of each new iteration as the process may produce unknown effects. To this end, an advanced hybrid high temperature polymer matrix composite (HTPMC) and high temperature CMC will be tested in extreme environments to determine their interlaminar shear properties.

1.3 Thesis Objective

The objective of this research was to experimentally determine the interface strength of high temperature, hybrid HTPMCs, and the creep strength of high temperature CMCs at elevated temperatures. The material systems evaluated in this research were:

1. Material 1: HTPMC without stainless steel foil
2. Material 2: HTPMC with stainless steel foil
3. Material 3: Hi-Nicalon^{TM} SiC-B_4C CMC

Each material was machined from a panel to create individual coupons for testing. Double notch-shear tests were conducted on both HTPMC and CMC materials. Materials 1 and 2 were tested at an elevated temperature of 204°C. Material 3 was tested at an elevated temperature of 1300°C in air and in steam. Compression testing was used for both HTPMC and CMC materials to determine the thermomechanical properties.

1.4 Methodology

The key objectives outlined above were achieved as follows:

1. Perform compression to failure tests or creep tests on double notch-shear specimens at elevated temperatures

2. Compare results obtained for different material systems and assess whether there was a marked improvement in one material system over the other or previous testing.

3. Examine tested specimens under an optical microscope and/or a Scanning Electron Microscope (SEM) to assess damage and failure mechanisms.

II. Background

This chapter offers a brief overview of composites, certain composite failure modes, and potential methods for avoiding these failure modes.

2.1 Composite Basics

A composite is a multiphase system that consists of two or more different constituents that, when combined, enhance the overall properties of the entire material[4]. The most basic composites consist of a reinforcement material and a matrix phase. The reinforcement material is generally found in one the following forms: continuous fibers, randomly aligned discontinuous/whisker fibers, particles, or braided/woven fibers (see Figure 3). The fibers and the matrix have distinct roles for enhancing the overall composite properties. The primary objective of the fibers is to carry the principal loads of the material. The matrix phase holds together the reinforcement material, transfers the load between fibers, and protects the fibers from the environment. The fibers can be oriented in any, in-plane direction as required for the load application. Fiber orientation can be arranged in an unidirectional orientation (all the fibers are aligned in one direction), a bidirectional orientation (fibers run in two directions, usually normal to each other), or a multidirectional orientation (fibers routed in more

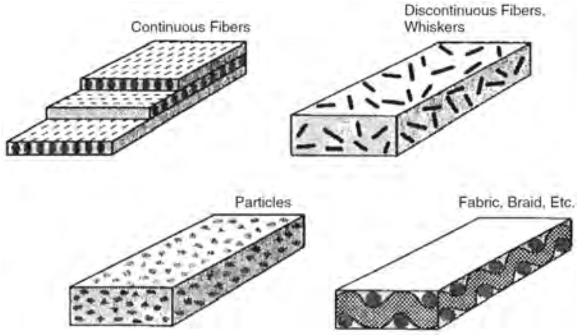

Figure 3. Types of Reinforcement Materials. Figure from [2]

than two directions)[5]. The mechanical properties and chemical reactions between the fibers and the matrix must be known and accounted for when creating a composite in order for the material to function properly. These phenomenons must be considered for the operating environments and loading conditions of the component throughout the entirety of its life.

Together, one layer of fibers and matrix is referred to as a ply or lamina. These individual plies can then be stacked to increase the mechanical properties of the overall composite or laminate, as seen in Figure 4. The reinforcement fiber orientations can vary within each ply or from layer to layer which makes up the composite's stacking sequence. The stacking sequence of Figure 4 consists of three unidirectional plies stacked in three different orientations. The optimal number of plies and their orientation/s can be vary depending on the design requirements.

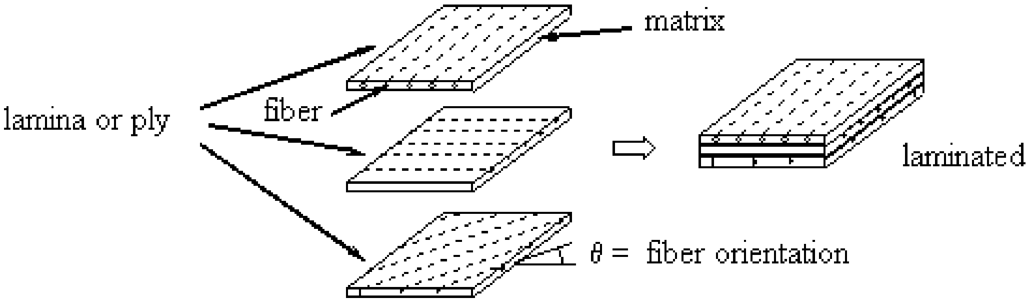

Figure 4. Laminated Composite Example. Figure from [6]

2.2 Common Failure Modes of CMCs and PMCs

Each classification of composite mentioned in Figure 2 introduce some weaknesses that are unique to its classification and some weaknesses that are shared across all composite materials. These weaknesses that can cause or accelerate the failure of a composite structure. While composites are generally desired for their high strength-to-weight ratio, some inherent disadvantages often include weak interlaminar shear strength (ILSS), low damage tolerance, and poor through-thickness strength when compared to metal alternatives[7]. As evolving technology continues to push the limits of existing composite materials, new techniques and materials must be developed to address these weaknesses while retaining the favorable properties. Some of the failure modes pertinent to the materials and experiments performed for this research effort are the subject of this section.

Although composites offer great potential, achieving the desired mechanical properties is often complex and requires extensive experimentation. Selecting fibers and matrix based purely on their individual performance may not yield the expected result without first understanding how the two phases work in concert. The behavior of the interfacial bond should be known and established fully before the initial layup and processing, through the entire limits of the operating environment and loading conditions while the structure is in service, and finally, over the expected life of the composite. Unwanted stresses and strains can be introduced to the matrix during the curing process which ultimately can introduce fatal flaws into the composite before it is placed into service[8]. Also, the bond between the fibers and matrix can change or degrade over time and this must be understood before the composite is used on a structural application. One aspect to understanding the total strength parameters of the overall composite is knowing how the composite behaves at the onset of failure and when the composite ultimately fails. The desire to control the toughness of composite is strongly influenced by the interfacial bond of the two phases. Additionally, the mismatch of the Poisson's ratio between the fiber and matrix can negatively impact the interfacial bond under various environmental and loading conditions[9]. As the composite is loaded near its yield point, the desired outcome is to have the fibers and matrix to fail in a gradual manner, known as graceful failure. The interfacial bond is a primary way to produce graceful failure. By creating an interfacial bond that is too strong, a crack will not be able to propagate through the composite and brittle fracture will occur. Therefore, a relatively weak interfacial bond is preferred to increase fracture toughness. Conversely, by having an interfacial bond that is too weak, debonding will occur between the fiber and matrix and the material will fail prematurely. Hence, accounting for interfacial bond is a preliminary design consideration when selecting a matrix and fiber combination.

Weak interlaminar shear strength results from inherent weaknesses in regard to low shear strength between adjoining lamina. Shear failure is a Mode II crack failure as shown by Figure 5. There are many contributors to low ILSS such as free edge effects, structural voids or discontinuities in the matrix, flaws/damage induced during manufacturing, and environmental effects[10]. These contributors can be the sole source of structural failure or they can work in concert to allow the part to fail. As with the interfacial bond of fibers and matrix, the bond strength of adjoining laminas is a balance between having enough strength to hold the plies together but still be weak enough to transmit cracks and produce graceful failure. The importance of proper adhesion between laminates cannot be understated, especially between dissimilar laminates, which will be covered in Hybrid Laminate Composite subsection (subsubsection 2.3.1.1).

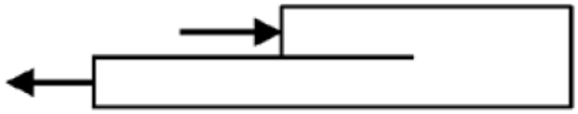

Figure 5. Shear - Mode II Crack Failure. Figure from [7]

An additional pitfall of composite materials relates to their anisotropic nature. Unlike metals, which are isotropic, the mechanical and physical properties of a composite can vary along different load directions in a three-dimensional space. This ultimately can lead to low through-thickness strength and weak bearing strength[8]. These shortcomings are plainly evident when loading composites in a manner for which it was not specifically designed. Any tensile or compressive load that is placed on the material that exceeds the load limit for that particular orientation will most likely cause damage. For example, this problem can lead to issues when it comes to tightening a fastener through a composite and compressing the material out-of-plane of the intended design. The conflicting requirements of fastener preload and preventing the laminate from being crushed is a common issue.

Finally, special care must be taken to ensure that defects are not introduced during manufacturing. Damaged fibers, unintended voids in the matrix, or contamination of either phase are just a few examples of things that can cause a composite to prematurely fail. New processing techniques for established composite constituents can produce unintended or unknown side effects. Manufacturing defects must be considered when a composite does not perform as expected.

2.3 Elevated Temperature Composites

Composites are very desirable materials for several applications but certain high temperature composites offer revolutionary gains in certain areas where current materials do not exist to meet unique applications. As mentioned previously, with the growing demand on the mechanical and physical properties of materials, increasing the material service temperature is a primary focus of composite designers. As shown in Figure 1, composites have low coefficients of thermal expansions when compared to steel and aluminum. For relatively low temperatures (350°C and below), HTPMCs have excellent strength-to-weight ratios (see Figure 6). The thermomechanical properties of any material can change as the temperature increases, which ultimately affects the mechanical properties and life of the material. All of these considerations culminate to further bolster the potential of composites in high temperature applications and fuel the demand for composite research at elevated temperatures.

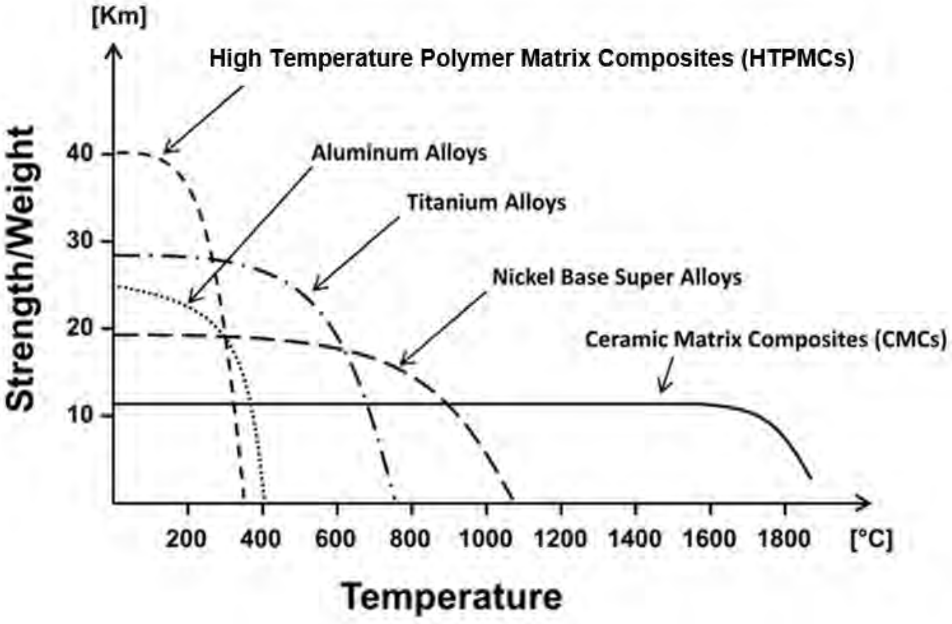

Figure 6. Strength-to-weight ratios as a function of operating temperatures for various materials. Figure from [11]

For operating temperatures above 350°C, however, a HTPMC's strength is drastically degraded and should not be utilized. For operating temperatures 350°C - 1500°C, CMCs should be considered. As evident in Figure 7, there is a large variance of service temperatures for polymers, alloys, and ceramics. However, there are clearly more design considerations than service temperature alone. Some of these considerations will be discussed in the following sections.

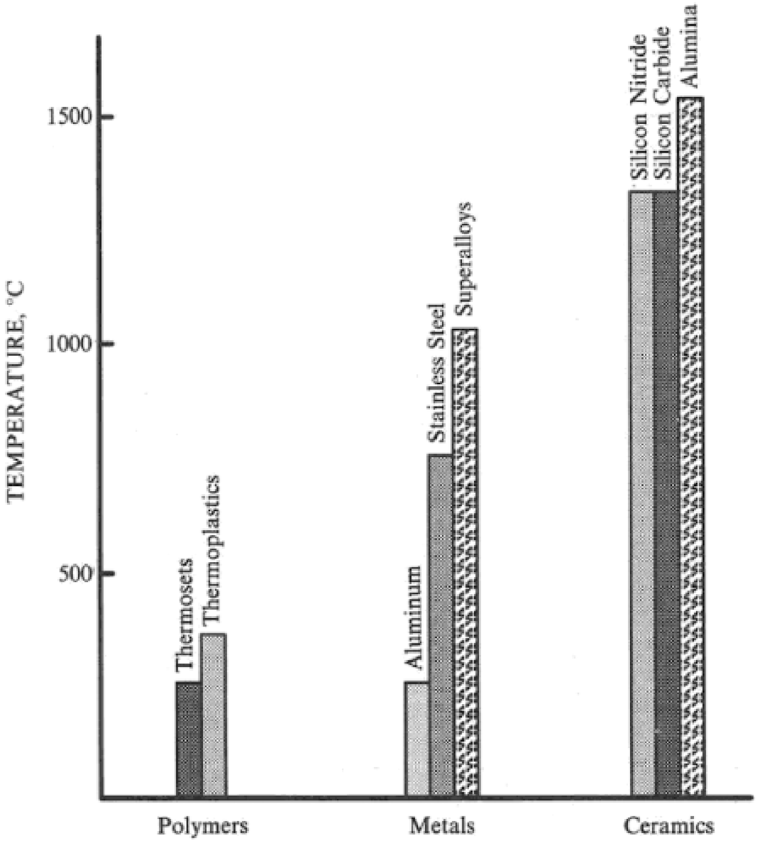

Figure 7. Service temperature limit of polymer, metals, and ceramics. Figure from [12]

2.3.1 Low Temperature Regime Composites.

As constituents have become more advanced and processing techniques are improved, they are now capable of operating in temperature regimes that have historically been reserved for specialized alloys. HTPMCs are being used in areas where operating temperatures approach 350°C. These HTPMCs exhibit excellent strength-to-weight ratios which allow designers to save additional weight on a component or redistribute the weight savings to other systems.

Generally, the matrix of a HTPMC is classified as a thermoplastic or thermosetting resin. Thermoplastic resins have the propensity to soften as the temperature increases but harden as the material cools. Alternatively, thermosetting resins retain their hardness as temperature increases due to covalent cross links that exist in their molecular makeup. However, as thermosetting resins reach their service temperature limit,they degrade and the polymer chains are destroyed[13]. Thermosetting resins can be classified as polyimides, polyesters, or epoxies. Polyester and epoxy resins currently have approximate service temperature limits of 100°C and 175°C, respectively, so they do not meet the needs of a HTPMC. Conversely, polyimides are stable at relatively high temperatures and are resistant to most chemicals[8].

2.3.1.1 Hybrid Laminate Composites.

One way to enhance the performance of composites is utilization of a combination of different reinforcement layers to create a hybrid laminate composite. Two areas where hybrid laminates offer potential improvement to the mechanical properties of composites address the bearing and shear strengths of the overall composite material. The marriage of the different layers is not a trivial endeavor and must be engineered in a way not to compromise the integrity of the composite. The intent of this research is to define the material properties and potential viability of a hybrid HTPMC.

The desire to improve the aforementioned failure modes of composites for HTPMCs opens the door to several potential strengthening methods. One way of addressing these deficiencies is a composite layup known as a hybrid laminate. A hybrid laminate consists of the usual fiber and matrix setup with another layer that specifically addresses the strength limitations of basic composites. Although this is not a novel concept, poor performance of previous hybrid laminate iterations has kept many proposed concepts from becoming completely viable.

Several iterations of hybrid metal laminates have been developed and tested in past years. One hybrid metal laminate approach is known as a Fiber Metal Laminate (FML).

Two examples of FML's are ARALL (Aramid Reinforced Aluminum Alloy Laminates) and GLARE (Glass Laminate Aluminum Reinforced Epoxy). ARALL was introduced in the early 1980's and consisted of uniaxial aramid fibers with intermediate adhesive layers of laminated sheet material[14]. Even though aramid fibers are known for their toughness, impact resistance, and creep resistance, they exhibit poor performance in compression[15] and in shear[16]. More critically, the interface strength between the aramid fibers and matrix material is easily compromised whenever moisture is introduced[17]. As a result of these inadequacies, ARALL was replaced in around 1990 by GLARE. GLARE consists of thin layers of 2024-T3 aluminum alloy and S2-glass fibers which are held together by the FM94 adhesive system[18]. The glass fibers used in GLARE offer better impact resistance, strength in compression, and adhesion to the metal laminate when compared to ARALL. However, GLARE's primary weakness is its low service temperature of approximately 100°C. This temperature regime is far below where other HTPMCs operate. Also, with the addition of moisture, the adhesive layers in between the laminae start to breakdown around 80°C[18]. Therefore, GLARE will not meet the needs of the design requirements for HTPMCs operating in harsh environments.

Emerging technology and materials have the potential to offer high temperature performance while avoiding the pitfalls of previous hybrid laminate composites.

2.3.2 High Temperature Regime Composites.

For temperatures above 350°C, CMCs exhibit excellent material properties. Some of these properties include superior strength, high stiffness, chemical inertness, and electrical resistance[1]. Additionally, the low density of CMCs offers a tremendous advantage when compared to the specialized alloys. One of the inherent flaws of ceramic materials is brittle behavior and low fracture toughness. Addressing this issue is the main focus of current CMC research and development. Graceful failure of CMCs is achieved by allowing energy to dissipate through the composite in way that promotes progressive failure. Crack deflection, fiber coating, and weak matrices are a few ways to facilitate graceful failure.

Great emphasis is placed on the mechanical properties of the interface of CMCs. Considerable care must be taken when designing and fabricating CMCs in order to reduce the introduction of unintended flaws. The interface is where many of the toughening mechanisms are employed to make CMCs more damage tolerant. Figure 8 illustrates the desired stress strain curve of damage tolerant CMCs. This behavior is not common for purely ceramic materials but the interface between the matrix and fibers allows for graceful failure.

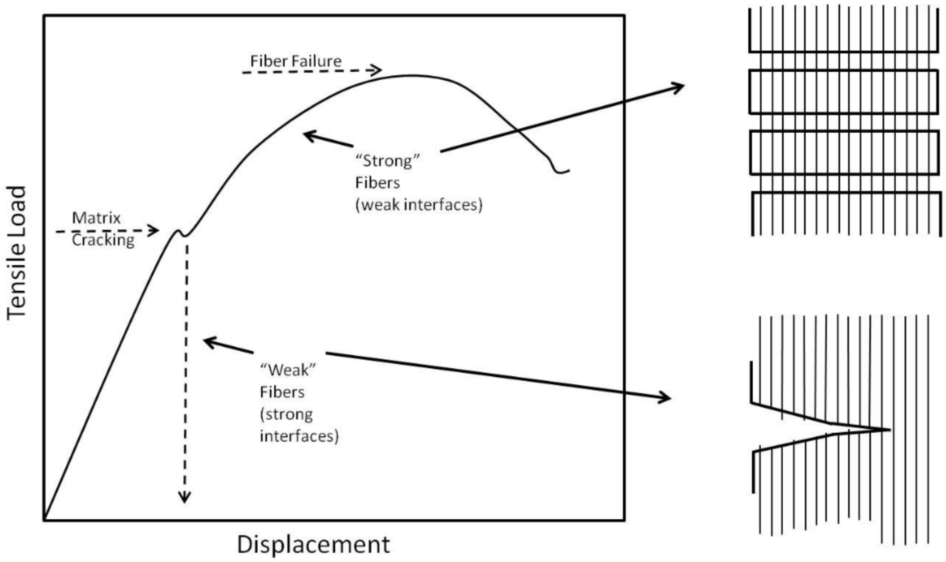

Figure 8. Stress strain curve of CMC with damage tolerant behavior. Figure from [19]

2.4 Previous Research of ILSS of SiC/SiC CMC

Choi et al[20, 21] evaluated the Interlaminar Shear properties of several different CMCs at high temperatures using double-notch shear (DNS) specimens. Choi and his colleagues performed ILSS and constant stress-rate tests in laboratory air. They also developed a phenomenological model and validated said model with the high temperature testing results.

A previous study of this CMC was accomplished by Pope[19] and these specific CMC specimens come from the same batch of materials as tested by Pope. Pope performed elevated temperature ILSS testing at 1200°C in both air and in steam environments. Compression testing of the CMC produced an average interlaminar shear strength of 27.2 MPa and an average compressive failure strain of 0.149%. Pope also performed creep testing in both air and steam which yielded interlaminar shear stresses anywhere from 16 to 22 MPa and also showed evidence of primary and secondary creep. Pope reported "The presence of steam only moderately affects creep lifetimes and larger creep strains are accumulated in steam than in air. At 18 MPa ($\approx$ 66% ILSS), steam decreased creep life by $\approx$ 12% and increased strain by $\approx$ 0.17%. At 20 MPa ($\approx$ 74% ILSS), the presence of steam decreased creep life by $\approx$ 28% and increased strain by $\approx$ 0.13%. However, at 22 MPa ($\approx$ 80% ILSS), the presence of steam actually increased creep life by $\approx$ 123% and increased strain by $\approx$ 0.06% above that observed in air." Pope observed in-ply delamination and matrix damage as the primary causes of failure for creep tests less than 26 hours and fiber failure as the primary cause of failure for tests longer than 26 hours[19].

The promising results of the experiments performed by Pope and Choi have spawned interest on the performance of this SiC/SiC CMC at higher temperatures.

III. Materials and Test Specimens

This chapter describes the materials researched, as well as the test material geometry.

3.1 Materials

Two types of composites were tested in this research effort. The first type was a HTPMC, which had two variants: one with a stainless steel foil located at the midsection and one without foil. The second type of composite that was tested was a CMC. Both types of composites were tested at elevated temperatures with a focus on the interlaminar shear properties of the HTPMC material and creep behavior in interlaminar shear for the CMC material.

3.1.1 Polymer matrix composite.

The two variants of HTPMC material were constructed in a similar manner. The composite material consisted of an AFR-PE-4 polyimide resin reinforced with 22 plies of an 8-harness-satin-weave Astroquartz-III pre-impregnated glass fabric. AFR-PE-4 is a high-temperature thermosetting polyimide resin manufactured by Renegade Materials Corporation (Springboro, OH). The first variant was a hybrid composite which, contained a 0.007-in (0.1778-mm) thick layer of AISI type 304 stainless steel. In this composite, the fiber orientation was aligned with the rolled direction of the stainless steel foil. The stainless steel foil was bonded to the adjoining composite laminae by polyimide adhesive FM 57. The addition of the stainless steel foil poses to increases bearing strength and fracture toughness of the HTPMC. These desirable attributes offer to greatly benefit composite structures where holes or fasteners are located. The second variant was a HTPMC consisting of the same fiber and matrix materials as the first hybrid composite. However, this HTPMC did not contain the stainless steel foil or polyimide adhesive. Composite panels of both variants were laid-up individually and then cured in an autoclave.

Each variant of the composite material was supplied in a form of a 12 in. x 6 in. (305 mm x 152 mm) panel. Panel thickness was approximately 4 mm for the hybrid HTPMC containing the stainless steel foil and the HTPMC without the stainless steel foil.

3.1.2 Ceramic Matrix Composite.

The ceramic matrix composite (CMC) studied in this work was Hi-Nicalon^{TM} SiC-B_4C (Hi-N/SiC-B_4C) fabricated by Hyper-Therm High-Temperature Composites, Inc. (Huntington Beach, CA). The CMC was reinforced with Hi-Nicalon^{TM} fibers woven in a five-harness satin weave, and was processed by chemical vapor infiltration (CVI). The Hi-Nicalon^{TM} fibers are the second generation of SiC fibers. They exhibit improved stiffness ($\approx$ 35%) and strength at higher temperatures compared to the first generation SiC fibers[19]. The Hi-Nicalon^{TM} fibers provide excellent creep resistance at temperatures up to 1200°C and when heat treated, show sufficient creep resistance up to 1600°C. The matrix consists of alternating layers of silicon carbide (SiC) and boron carbide (B_4C). Laminated fiber preforms were produced from 18 plies of woven fabric in a 0/90 layup symmetric about the mid-plane with warp and fill plies alternated. Prior to infiltration, the preforms were coated with pyrolytic carbon fiber coating ($\approx$ 0.40 μm thick) with boron carbide overlay ($\approx$ 1.0 μm thick) to decrease bonding between fibers and matrix. The composite had a finished fiber volume of 36.4% and a density of $\approx$ 2.40 g/cm^3. The CMC was supplied in a form of two 5 mm thick panels.

For this CMC, silicon carbide and boron carbide are added in alternating layers to help create a “self healing matrix.” In this composite, the self-healing occurs when boron carbide reacts with oxygen at elevated temperature to produce a liquid oxide phase. When this composite is subjected to mechanical loading at elevated temperature, matrix cracks initiate on the composite surface. The matrix cracks allow oxygen to diffuse into the material until it encounters the boron carbide and reacts with boron carbide. The reaction product is a liquid phase which flows into the cracks, effectively closing the matrix cracks. Once the crack is filled by the liquid phase, the diffusion of oxygen is impeded. Oxygen is prevented from reaching oxidation - prone fibers. As a result, environmental durability of the composite is significantly improved[19]. The composite microstructure is shown in Figure 9.

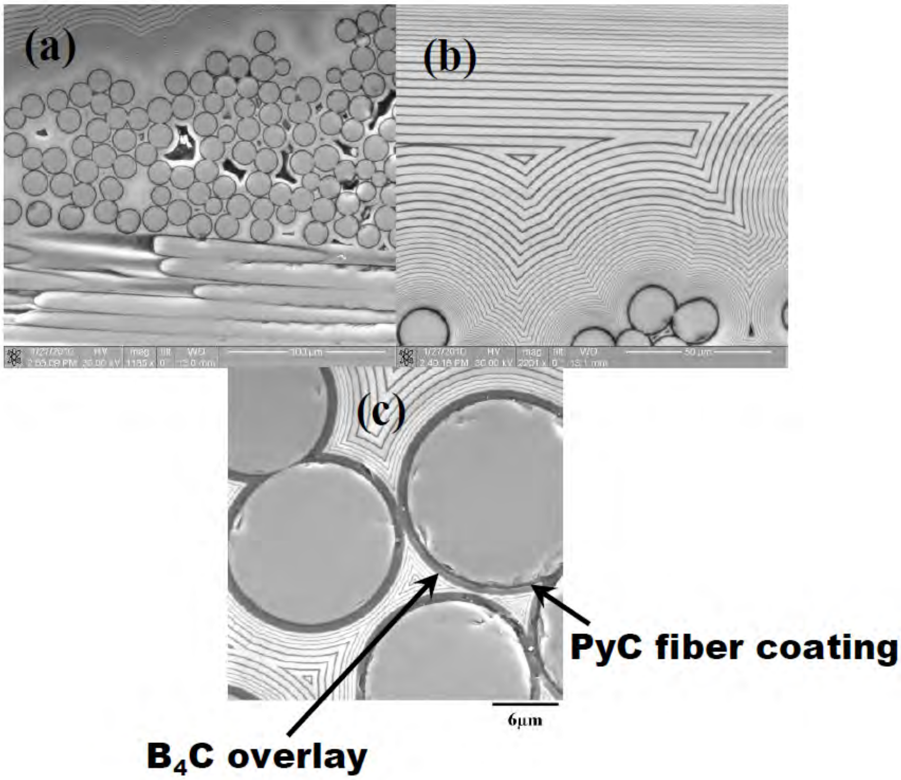

Figure 9. SEM micrographs showing: (a) typical microstructure of Hi-Nicalon^{TM} SiC-B$_4$C (Hi-N/SiC-B$_4$C) ceramic composite, (b) oxidation inhibited matrix consisting of alternating layers of SiC and B$_4$C, (c) fibers and PyC fiber coating with B$_4$C overlay[19]

3.2 Specimen Geometry and Preparation

The behavior of both variants of the HTPMC material, as well as that of the CMC material, were studied using double-notch shear test specimens. All test specimens were cut from the composite panels using diamond grinding. For both variants of the HTPMC material, test specimens were approximately 150 mm long, 18 mm wide, and 4 mm thick. Figure 10, displays side views of both DNS HTPMC variants. The CMC test specimens were approximately 150 mm long, 15 mm wide, and 5.5 mm thick. The CMC test specimens were also sealed with a CVI SiC overcoat after machining. The notches of 0.5-mm width were extended to the middle of each test specimen within ±0.05 mm so that shear failure occurred on the plane between the notch tips. The distance between the notches was 13 mm.

Figure 10. Top: HTPMC without stainless steel foil
Bottom: HTPMC with stainless steel foil

The DNS test specimens were designed following the guidance in the ASTM C1425[22], yet the dimensions of the DNS specimens used in this work were different from those specified in the standard. Specimen geometry and dimensions are shown in Figure 11. The 13-mm distance between the notches was chosen specifically to enable the measurement of compressive strain between the notch tips with an MTS high-temperature extensometer of 12.5-mm gage length. The overall specimen length of 150 mm ensures that the local stress fields at the notch tips are not influenced by the external loading at the specimen ends. Schematic in Figure 12 shows how the DNS specimens are loaded in compression in order to induce interlaminar shear along the midplane. The ILSS is calculated using the failure load and the known dimensions of the tested specimens.

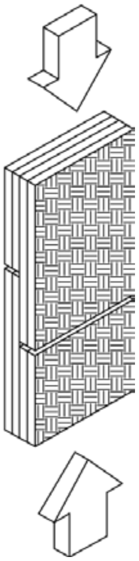

Figure 11. Schematic of Compression of Double-Notched Test Specimen[22]

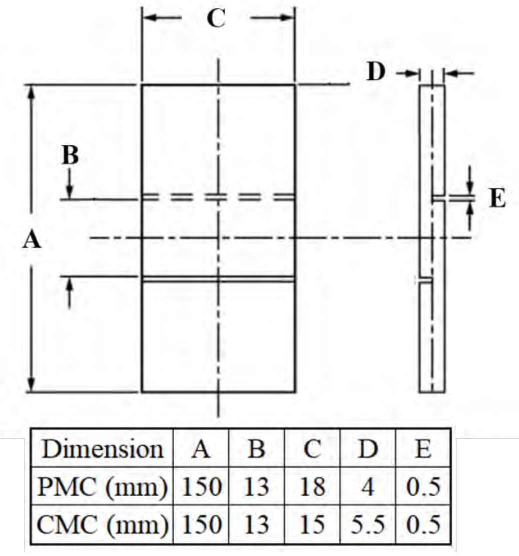

Dimension	A	B	C	D	E
PMC (mm)	150	13	18	4	0.5
CMC (mm)	150	13	15	5.5	0.5

Figure 12. Dimensions for the DNS HTPMC and CMC specimens. Adapted from[22]

Fiberglass tabs were affixed to the gripping sections of all test specimens to prevent damage from the wedge grips of the testing machine. The fiberglass tabs were bonded to the specimens using M-Bond 200 adhesive. The fiberglass tabs were then marked with the specimen identifier, as well as top/bottom and left/right, depending on how the specimen was to be loaded into the testing machine.

IV. Experimental Setup and Testing Procedures

This section describes the testing equipment and test procedures, as well as the used for microstructural examination.

4.1 Experimental Setup

All tests were performed using MTS 810 servo-controlled testing machines equipped with hydraulic water-cooled wedge grips. A testing machine with 3 kip (Figure 13) capacity was used to test HTPMC specimens and a testing machine with 5 kip capacity (Figure 14), to test CMC specimens. A MTS Flex Test 40 digital controller was used to generate input signals and to collect test data. Strain measurement was accomplished with a MTS Model 632.53E-14 uniaxial high-temperature, low-contact-force extensometer with a 12.5-mm gage length. The extensometer extension rods were positioned as close to the notch roots of the DNS specimen as possible (see Figure 15).

Figure 15. Extensometer Contact Locations (red dots)

A compact two-zone resistance furnace and two MTS 409.83 temperature controllers were used for testing CMC specimens at elevated temperature, whereas a single zone

Figure 13. 3 Kip MTS Machine used for HTPMC Testing

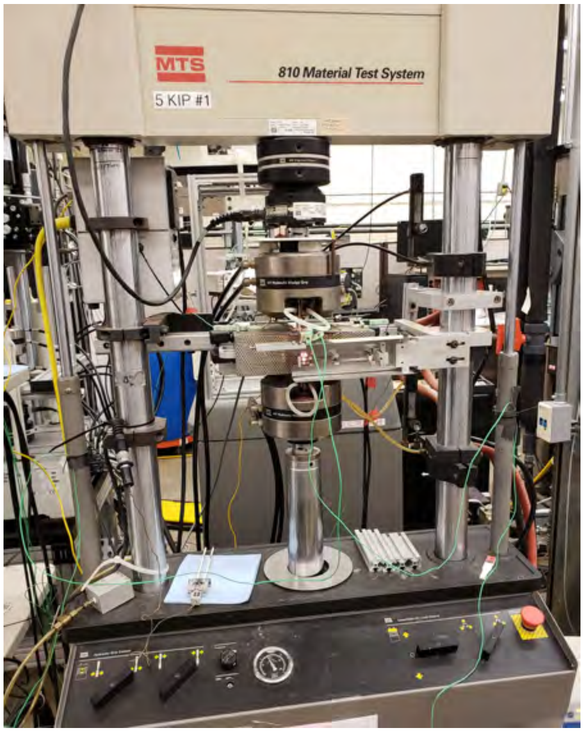

Figure 14. 5 Kip MTS Machine used for CMC Testing

resistance furnace and a single MTS 409.83 temperature controller were employed to test HTPMC specimens. Thermo Scientific NESLAB RTE-7 Circulating Baths were employed to cool the grips by continuously pumping 15°C water through the grip wedges. The gripping surfaces of the wedges were also coated with Surfalloy to prevent specimen slippage. Grip pressure of 10 MPa was used to keep the test specimen in place.

Deionized water and an AMTECO steam generator (see Figure 16) were used to generate steam for testing in steam. Previous chemical analysis of water entering the steam generator revealed trace amounts (below 10 ppb) of Al, B, Fe, and Zn. Chemical analysis of condensed water exiting the steam generator revealed trace amounts (10-30 ppb) of Al, B, and Fe, and slightly higher but still negligible amounts (55-80 ppb) of Zn. We believe that these levels of impurities are too low to cause contamination of the test specimens and to influence the mechanical performance of the CMC studied in this work. Tests in steam also employed an alumina susceptor (see Figure 17) tube with end caps, which fit inside the furnace. The specimen gage section remains inside the susceptor, while the ends of the specimen pass through slots in the susceptor. Steam enters the susceptor through a feeding tube in a continuous stream with a slightly positive pressure, expelling the dry air and creating a near 100% steam environment inside the susceptor.

Figure 16. AMTECO Steam Generator

Figure 17. Alumina Susceptor

4.2 Temperature Calibration

The furnace controllers employed in this work use non-contacting thermocouples exposed to the ambient environment near the test specimen. Hence, the controller temperature set point is not necessarily the same as the target temperature of the test specimen. In order to determine furnace set points that would produce the target test temperature of the specimen, temperature calibration was performed. A test specimen was instrumented with two thermocouples, one bonded to each side of the specimen. The settings on the furnace controllers were adjusted until the desired temperature of the test specimen was achieved. The determined furnace settings were then used in actual tests. The furnace settings for testing in steam were determined by placing the specimen instrumented with thermocouples in steam and repeating the furnace calibration procedure. Temperature calibration was repeated periodically. Temperature calibration was also performed each time a heating element was replaced to verify that the furnace set points had not changed. During temperature calibration the testing machine must be placed in force control and a zero force command must be issued in order to avoid compressive loads on the specimen due to thermal expansion.

4.2.1 HTPMC Temperature Calibration.

The HTPMC specimens were tested using a single-zone, hot-rail furnace (see Figure 18) integrated with the 3 Kip MTS machine and a MTS 409.83 Temperature Controller. The target test temperature for HTPMC specimens (both variants) was 204°C. To calibrate the furnace controller, a HTPMC specimen was instrumented with two K-type thermocouples attached to each side of the specimen gage sections with high temperature Kapton tape and thin wire (see Figure 19). A separate temperature calibration procedure was performed for each variant of the HTPMC specimens (i.e. HTPMC specimens with and without stainless steel foil). During temperature calibration as well as during actual testing the temperature of the HTPMC specimens was increased at a rate of 2°C/min, as to not thermally shock the material.

Figure 18. Single-Zone Furnace for the 3 Kip Machine

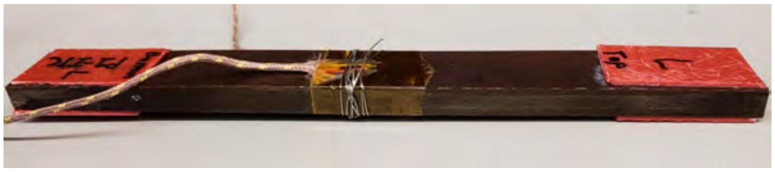

Figure 19. HTPMC (without foil) Temperature Calibration Specimen

4.2.2 CMC Temperature Calibration.

The CMC specimens were tested using a two-zone, hot-rail furnace integrated with the 5 Kip MTS machine and two MTS 409.83 Temperature Controllers. The target test temperature for CMC specimens was 1300°C. To calibrate the furnace controller, a CMC specimen was instrumented with two R-type thermocouples secured to each side of the specimen gage section with high temperature pieces of alumina and thin wire (see Figure 20). To achieve a repeatable temperature distribution along the specimen gage section, a ceramic susceptor, shown in Figure 17, was used in all tests of the CMC specimens. Therefore, during temperature calibration, the CMC specimen instrumented with thermocouples was encased in the susceptor as well. The furnace controller settings for testing at 1300°C in air were determined by performing temperature calibration in laboratory air. The furnace controller settings for testing in steam were determined by placing the specimen instrumented with thermocouples in steam environment and repeating the furnace calibration procedure. During temperature calibration, as well as during actual testing, the temperature of the CMC specimens were increased at a rate of 1°C/s. Since the target test temperature of 1300°C for the CMC specimens approached the maximum temperature capability of the furnace, the top and bottom of the furnace was insulated using Rescor ceramic blankets in order to minimize heat loss. Despite the additional insulation, furnace heating elements failed frequently. Temperature calibration procedure was repeated every time a heating element was replaced.

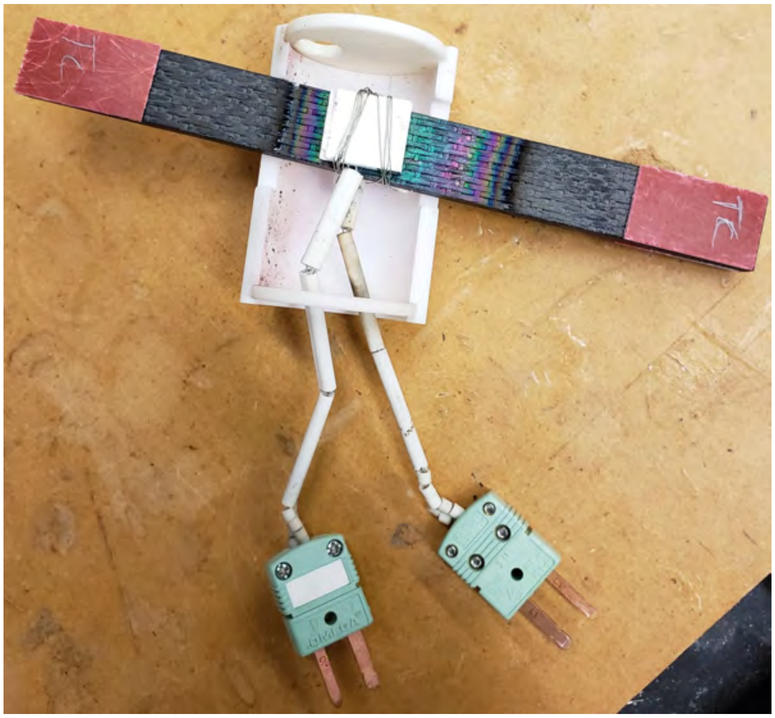

Figure 20. A CMC specimen instrumented with Two R-type Thermocouples for Temperature Calibration

4.3 Interlaminar Shear Testing

The test method used in this work was based on the ASTM Standard C1425[22]. In the case of the two HTPMC variants, the objective was to evaluate interlaminar shear properties, specifically the interlaminar shear strength (ILSS), in order to determine whether additional of the stainless steel foil was beneficial. In the case of the CMC, the study focused on the interlaminar shear properties and on creep behavior in interlaminar shear at the maximum use temperature for this CMC.

The DNS test specimen and test method outlined in the ASTM Standard C1425[22] were chosen over other common methods for determining ILSS, such as Short Beam Shear (SBS) tests or Iosipescu shear tests, for several reasons. The geometry of the DNS specimen allows the compressive loads to be transmitted only at the midplane and therefore produces more realistic ILSS values than the other test methods. To this point, SBS testing has been shown to produce a non-constant bending moment along the shear plane, which can negatively affect the measured strength[23]. Additionally, the shear stress distribution can vary throughout the length and width of the beam which can cause the maximum shear stress to not occur along the neutral axis[24]. Finally, the DNS test method permits a relatively simple approach for heating the specimen without damaging the testing equipment. In all tests, the shear stress, τ, between the notches along the shear plane was calculated according to the ASTM Standard C1425[22]. For both materials, the interlaminar shear stress was calculated with the fundamental equation for stress:

$$\tau = \frac{P}{Wh} \tag{4.1}$$

where P is the applied force, W is the specimen width, and h is the distance between the notches. While the shear stress distribution between the notches is not uniform, the average shear stresses provided by Equation 4.1 are useful when evaluating interlaminar shear strength and comparing creep behavior of specimens subjected to identical mechanical tests in different environments.

4.4 HTPMC Testing

The purpose of testing the two variants of the HTPMC material was to evaluate the ILSS of the HTPMC containing stainless steel foil and compare it to the ILSS of the HTPMC without the stainless steel foil. In testing the HTPMC with foil in the interlaminar shear, we essentially test the strength of the polyimide adhesive that joins the HTPMC to the stainless steel foil. The objective, of course, is to determine whether the selected adhesive performs well, thus making the addition of the foil beneficial.

The same procedures were used for testing both HTPMC variants. First, the test specimen was gripped in the testing machine and the furnace closed around the specimen. Then, the temperature was increased to the target test temperature of 204°C (400°F) at a rate of 2°C/min and held at 204°C for 30-45 min prior to mechanical loading being applied. During heat-up to and soak at 204°C, the testing machine was in force control under zero force command.

To measure the ILSS, a monotonic compression test to failure was performed in force control with the rate of 1080 N/s. Once failure was achieved, a failure detector included in the MTS program shut down the testing machine as well as the furnace. Correct programming of the failure detector was critical to preserve the fracture surfaces of the failed specimens. Otherwise, the two halves of the failed DNS specimens would fuse together under continued compressive loading.

A screenshot of the MTS program is shown in Figure 21.

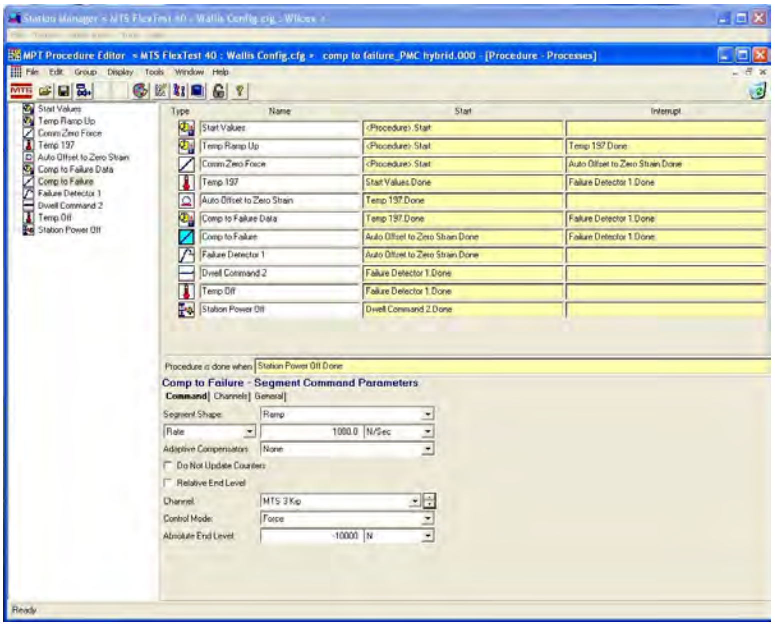

Type	Name	Start	Interrupt
	Start Values	<Procedure>.Start	
	Temp Ramp Up	<Procedure>.Start	Temp 197.Done
	Comm Zero Force	<Procedure>.Start	Auto Offset to Zero Strain.Done
	Temp 197	Start Values.Done	Failure Detector 1.Done
	Auto Offset to Zero Strain	Temp 197.Done	
	Comp to Failure Data	Temp 197.Done	Failure Detector 1.Done
	Comp to Failure	Auto Offset to Zero Strain.Done	Failure Detector 1.Done
	Failure Detector 1	Auto Offset to Zero Strain.Done	
	Dwell Command 2	Failure Detector 1.Done	
	Temp Off	Failure Detector 1.Done	
	Station Power Off	Dwell Command 2.Done	

Procedure is done when: Station Power Off.Done

Comp to Failure - Segment Command Parameters

Segment Shape: Ramp
Rate: 1000.0 N/Sec
Adaptive Compensators: None
☐ Do Not Update Counters
☐ Relative End Level
Channel: MTS 3 Kip
Control Mode: Force
Absolute End Level: -10000 N

Figure 21. Screenshot of MTS Test Procedure for Testing the HTPMC DNS Specimens in Compression to Failure

4.5 CMC Testing

The objective of the CMC testing was to evaluate the creep behavior in interlaminar shear of the selected composite at 1300°C in air and in steam. The CMC test specimen was heated to target test temperature of 1300°C at a rate of 1°C/s, then held at test temperature for 30-45 min before applying mechanical loading.

The present effort builds on the previous research effort by Pope[19], who evaluated creep in interlaminar shear of this composite at 1200°C in air and in steam. For this current effort, the monotonic compression test was performed at 1300°C to determine the ILSS at that temperature. The test procedure used in this test was similar to the procedure outlined above for testing the HTPMC specimens. However, the CMC specimen was loaded in force control with the rate of 1500 N/s to failure. The same loading rate was used to reach the desired creep stress level in creep tests. Creep run-out was defined as 100 h at creep stress. All specimens that achieved creep run-out were unloaded to zero load, then tested in compression to failure to measure the retained ILSS. The test procedures programmed for the monotonic compression test and for the creep test include a failure detector so that the testing system (both the hydraulics and the furnace) would shut down once specimen failure occurs. In the event of specimen failure, the bottom grip holding the bottom portion of the failed specimen would drift downwards, removing the bottom half of the failed specimen from the furnace, thus protecting the fracture surface from further oxidation.

4.6 Optical Microscope and Scanning Electron Microscope

Test specimens of all materials studied in this effort were examined before and after testing with a Zeiss Discovery stereoscopic optical microscope (see Figure 22).

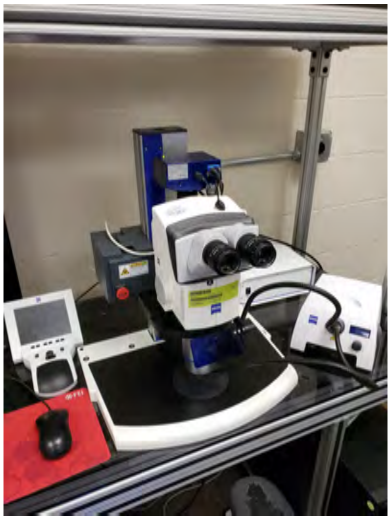

Figure 22. Zeiss Optical Microscope

The fracture surfaces of the CMC specimens were also examined using a TESCAN MAIA3 Scanning Electron Microscope (SEM) (see Figure 23). In preparation for SEM examination, the CMC specimens were cut approximately 0.5 in away from the fracture surface using a diamond-tipped saw. No coolant was used in order to avoid contamination of the fracture surface. Since the constituents of the CMC are conductive, no coating was required to prepare the samples for SEM examination.

Figure 23. TESCAN MAIA3 Scanning Electron Microscope

V. Results and Discussion

5.1 Thermal Expansion Coefficients

In all tests, strain was recorded during heating to test temperature as well during the soak at test temperature. Thus, the thermal strains produced by the HTPMC and the CMC specimens were measured in all tests. Assuming nominal room temperature to be 23°C, a coefficient of linear thermal expansion (CTE), α, was calculated for each test specimen as:

$$\alpha = \frac{\epsilon_t}{\Delta T} \tag{5.1}$$

where ϵ_t is the measured thermal strain (m/m) and ΔT is the temperature change. The temperature change was 23°C to 204°C for HTPMC testing and 23°C to 1300°C for the CMC testing. Thermal strains and CTE results for HTPMC and CMC materials are shown in Table 1 and Table 2, respectively. Note, the CTE values for the HTPMC containing the foil were approximately twice as large as the HTPMC without the foil. The CMC thermal strains and CTE observed values at 1300°C were similar to the values recorded by Pope[19] (see Table 3).

Table 1. Thermal Strain and Coefficient of Linear Thermal Expansion Obtained for HTPMC Specimens with and without Stainless Steel Foil

Specimen	Thermal Strain (%)	Coefficient of Linear Thermal Expansion, α(10^{-6}/°C)
Non-Hybrid HTPMC		
P1-3	0.16	9.80
P1-4	0.11	6.84
P1-5	0.10	5.81
Average	0.12	7.48
Std Dev	0.03	2.07
Hybrid HTPMC		
P2-3	0.27	15.58
P2-4	0.25	14.40
P2-5	0.25	14.59
Average	0.26	14.86
Std Dev	0.01	0.63

Table 2. Thermal Strain and Coefficient of Linear Thermal Expansion Properties for Hi-Nicalon^{TM} SiC-B$_4$C Specimens

Specimen	Thermal Strain (%)	Coefficient of Linear Thermal Expansion, $\alpha(10^{-6}/^{\circ}C)$
CMC1	0.47	3.71
CMC2	0.49	3.84
CMC3	0.50	3.94
CMC4	0.55	4.31
CMC5	0.52	4.07
CMC7	0.55	4.27
CMC9	0.54	4.23
Average	0.52	4.05
Std Dev	0.03	0.23

Table 3. Thermal Strain and Coefficient of Linear Thermal Expansion Properties for Hi-Nicalon^{TM} SiC-B$_4$C Specimens. Data from Pope[19]

Specimen	Thermal Strain (%)	Coefficient of Linear Thermal Expansion, $\alpha(10^{-6}/^{\circ}C)$
Pope1	0.54	4.55
Pope2	0.47	4.03
Pope3	0.54	4.57
Pope4	0.52	4.42
Pope5	0.48	4.12
Pope6	0.53	4.53
Pope7	0.51	4.31
Average	0.51	4.36
Std Dev	0.03	0.22

5.2 HTPMC - Interlaminar Shear Strength

Both variants of HTPMC materials were tested in monotonic compression to failure at 204°C to determine ILSS. The tests were performed in stress control at a rate of 5 MPa/s. Time, displacement, strain, force command, force feedback, and furnace temperature were recorded in each test. These parameters, along with the specimen dimensions, were used to calculate the interlaminar shear stresses for all test specimens. The ILSS values of the HTPMC without the stainless steel foil are consistent with reported test data by Whitley[25] for AFR-PE-4 with similar test conditions. Interlaminar shear stress-compressive strain curves are presented in Figure 24. The test results are also summarized in Table 4. Results in Table 4 and Figure 24 reveal that the addition of stainless steel foil degraded the ILSS of the HTPMC by 58% on average.

We attribute the low ILSS values of the hybrid HTPMC with stainless steel foil to poor performance of the polyimide adhesive that was used to bond stainless steel foil to the HTPMC plies. We do not believe that further testing of this material system will produce useful results. Alternate methods of fabricating HTPMC with stainless steel foil should be explored.

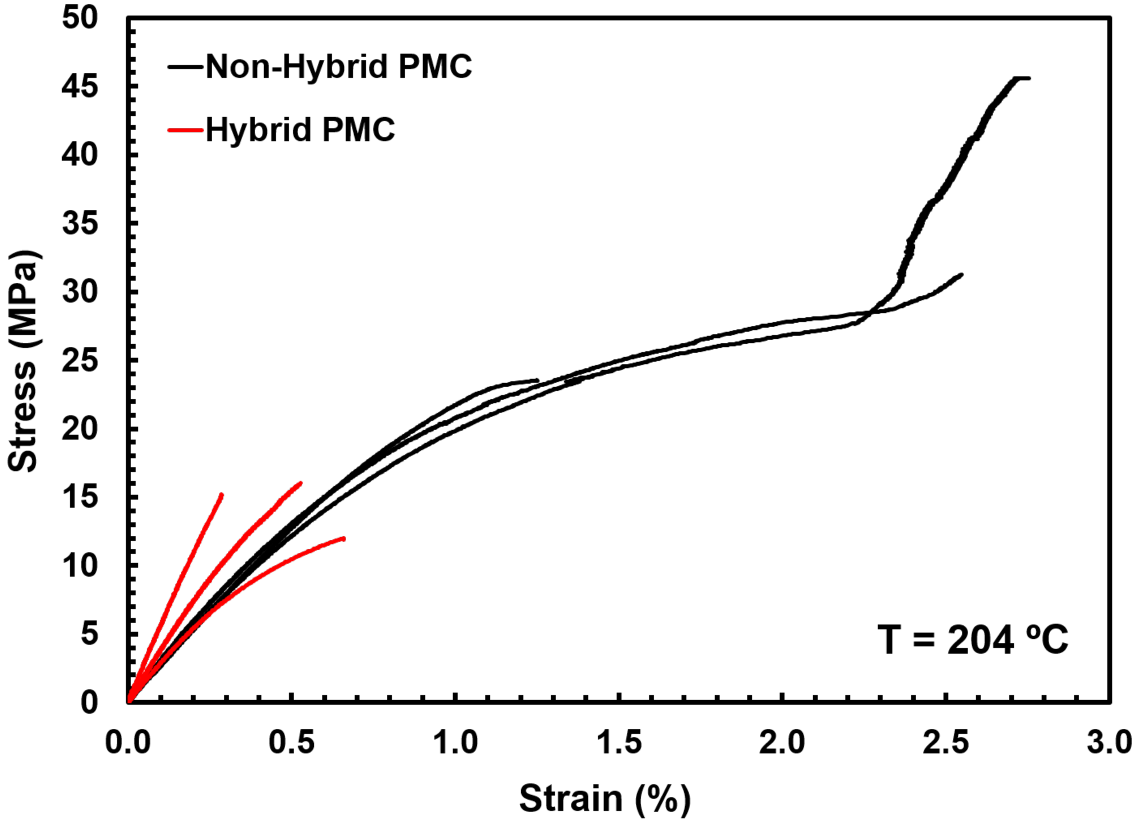

Figure 24. Interlaminar Shear Stress vs. Compressive Strain Curves obtained for HTPMC and for Hybrid HTPMC containing stainless steel foil at 204°C in air

Table 4. Interlaminar Shear Strength and Compressive Failure Strain obtained for HTPMC and Hybrid HTPMC containing Stainless Steel Foil at 204°C in Laboratory Air

Specimen	ILSS (MPa)	Compressive Failure Strain (%)
HTPMC		
P1-3	24	1.249
P1-4	46	2.722
P1-5	31	2.535
Average	33	2.168
Std Dev	11.2	0.802
Hybrid HTPMC containing stainless steel foil		
P2-3	15	0.286
P2-4	16	0.528
P2-5	12	0.658
Average	14	0.491
Std Dev	2.2	0.189

5.3 CMC - Interlaminar Shear Strength

The ILSS of Hi-Nicalon^{TM} SiC-B_4C CMC was measured at 1300°C in air in compression to failure testing of the DNS specimens. These tests were performed in stress control at a rate of 8 MPa/s. Time, displacement, strain, force command, force feedback, and furnace temperature were recorded in all tests. This data was used to calculate interlaminar shear stresses for all test specimens. Values of the ILSS and compressive failure strain obtained at 1300°C are summarized in Table 5, where the results obtained at 1200°C by Pope[19] are included for comparison. The interlaminar shear stress - compressive strain curves are presented in Figure 25.

Results in Figure 25 demonstrate that the interlaminar shear stress vs. compressive strain behavior obtained at 1300°C is qualitatively similar to that produced at 1200°C. Typical interlaminar shear stress vs. compressive strain curves produced at 1200°C and 1300°C are nearly linear until failure occurs. The average ILSS was 23 MPa at 1300°C and 27.2 MPa at 1200°C[19]. Not surprisingly, an increase in temperature from 1200°C to 1300°C caused a 15% loss of ILSS. The ILSS values obtained in this work are consistent with the ILSS values of 20-30 MPa obtained by Choi et al[20] for a 2D woven Hi-Nicalon/SiC composite at 1316°C in air.

Table 5. Interlaminar shear strength and compressive failure strain obtained for Hi-Nicalon^{TM} SiC-B$_4$C CMC at 1200°C and 1300°C in air. Data at 1200°C from Pope[19]

Specimen	ILSS (MPa)	Compressive Failure Strain (%)
1200 °C		
Pope1	27	0.153
Pope2	28	0.154
Pope3	27	0.115
Pope4	27	0.172
1300 °C		
CMC7	22	0.162
CMC8	24	0.099

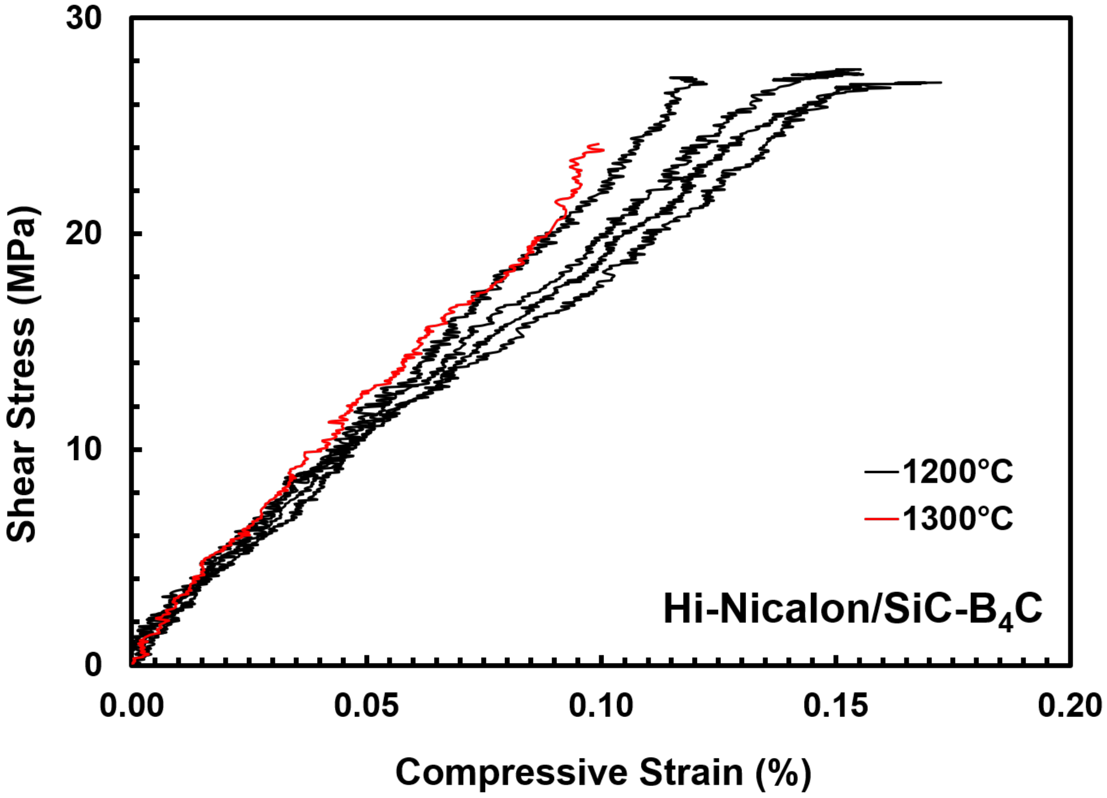

Figure 25. Interlaminar Shear Stress vs. Compressive Strain curves obtained for Hi-Nicalon^{TM} SiC-B$_4$C CMC at 1200°C and 1300°C. Data at 1200°C from Pope[19]

5.4 CMC - Creep in Interlaminar Shear

Creep-rupture tests were performed at 1300°C in air and in steam at shear stress levels ranging from 13 MPa (57% ILSS) to 20 MPa (87% ILSS). Creep rupture results obtained at 1300°C in air and in steam are summarized in Table 6 and Table 7, respectively. Creep-rupture results at 1200°C from prior work [19] are included in Table 6 and Table 7 for comparison.

Table 6. CMC Creep Rates in Air at 1200°C Pope[19] and 1300°C

Stress (MPa)	Creep Rate (s^{-1})
1200°C in Air	
16	5.82E-10
18	1.58E-09
18	1.82E-09
20	1.77E-08
20	1.15E-08
22	3.28E-08
22	1.95E-08
1300°C in Air	
13	1.08E-09
15	4.34E-09
16	5.27E-08
18	1.51E-07
20	2.80E-07

Table 7. CMC Creep Rates in Steam at 1200°C Pope[19] and 1300°C

Stress (MPa)	Creep Rate (s^{-1})
1200°C in Steam	
16	1.91E-09
18	2.80E-09
18	3.1E-09
20	2.07E-08
20	1.58E-08
22	2.63E-08
22	2.27E-08
1300°C in Steam	
13	2.61E-09
15	1.01E-08
20	1.81E-07

Typical creep strain vs. time curves obtained at 1300°C in air and in steam are shown in Figure 26. All creep curves exhibited of primary and secondary creep regimes but no tertiary creep. At 1300°C in air, creep run-out of 100 h is achieved at the shear stress of 13 MPa (57% ILSS). Creep strains accumulated at 13 MPa in air are comparable to the failure strains obtained in compression tests. Creep strains accumulated at stresses above 15 MPa considerably exceed failure strains produced in compression tests. Steam had virtually no effect on the creep run-out stress. Creep run-out was achieved at 13 MPa in steam as well as in air. However, larger creep strains are accumulated in steam than in air.

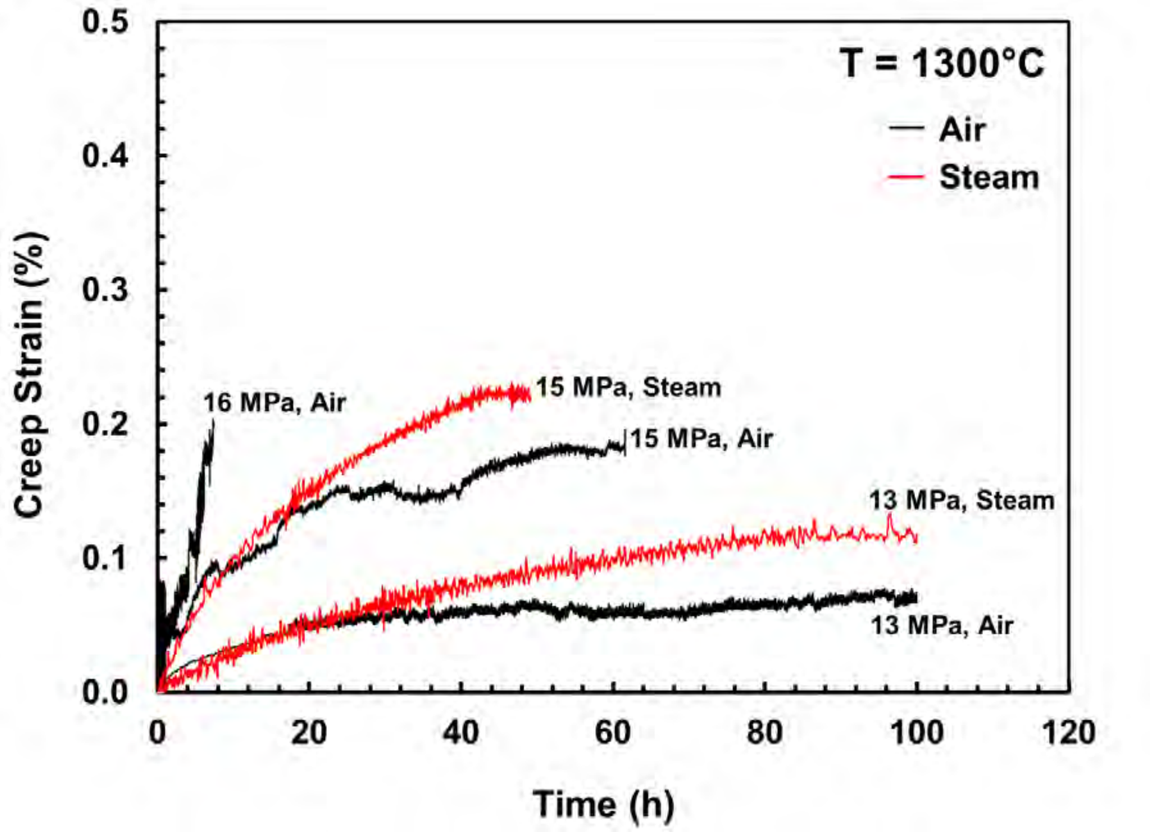

Figure 26. Creep strain vs time curves for Hi-Nicalon^{TM}/SiC-B_4C CMC obtained at applied interlaminar shear stresses in the 13-16 MPa range at 1300°C in air and in steam

Creep strain vs. time curves obtained for Hi-Nicalon^{TM} SiC-B_4C CMC at 1300°C in air are also shown in Figure 27, where creep curves at 1200°C in air from Pope [19] are included for comparison.

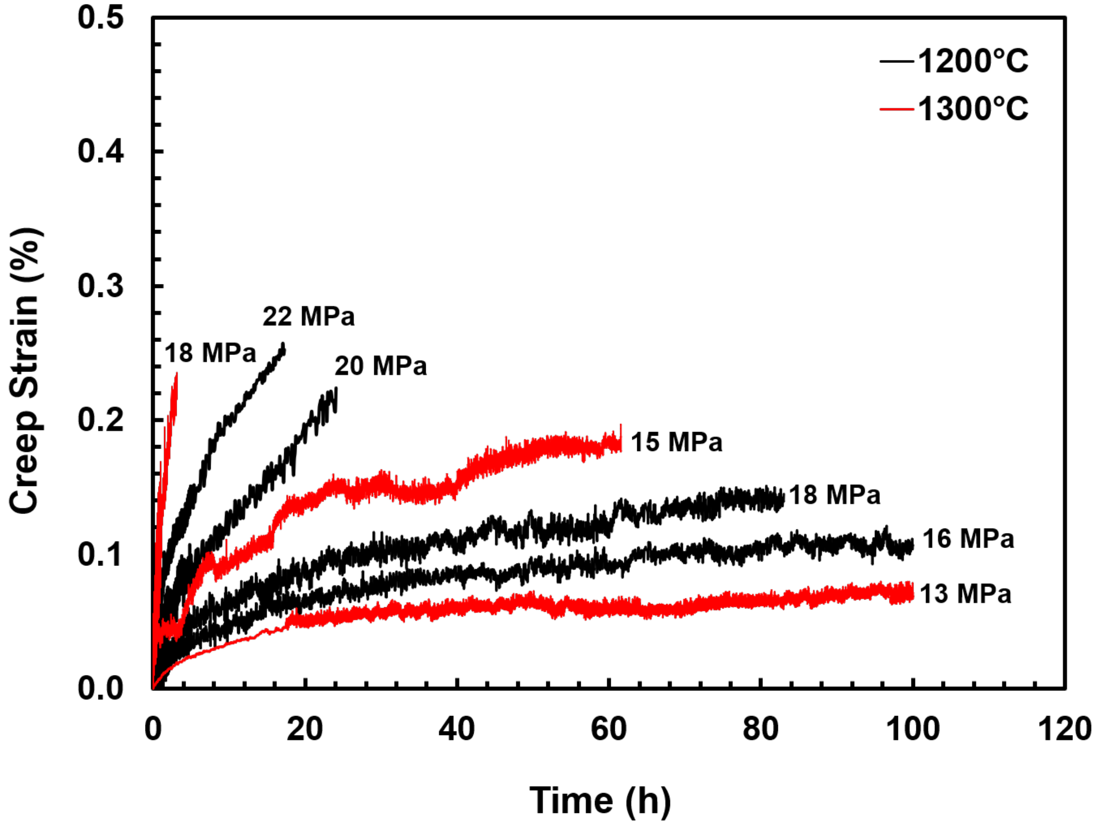

Figure 27. Creep strain vs time curves for Hi-Nicalon™ SiC-B_4C CMC obtained at 1200°C and 1300°C in air. Data at 1200°C from Pope[19]

Results in Figure 27 demonstrate that increasing the temperature from 1200°C to 1300°C had a degrading effect on creep performance of the composite in air. Creep strains accumulated at 1300°C are significantly higher than those accumulated at 1200°C. The increase in creep rates as a function of temperature are attributed to the degradation of fibers and interfacial sliding resistance[26]. In contrast, creep lifetimes produced at 1300°C are considerably shorter than those produced at 1200°C. For example, consider creep tests performed at 16 MPa at 1200°C and those performed at 15 MPa at 1300°C. While creep run-out of 100 h was achieved at 16 MPa at 1200°C, specimen tested at 15 MPa at 1300°C survived only 61.5 h.

Creep strain vs. time curves obtained for Hi-Nicalon™ SiC-B_4C CMC at 1300°C in steam are also shown in Figure 28, where creep curves at 1200°C in air from prior work [19] are included for comparison. As in air, in steam considerably larger creep strains are produced at 1300°C than at 1200°C. In steam, creep lifetimes produced at 1300°C are also much shorter than those produced at 1200°C.

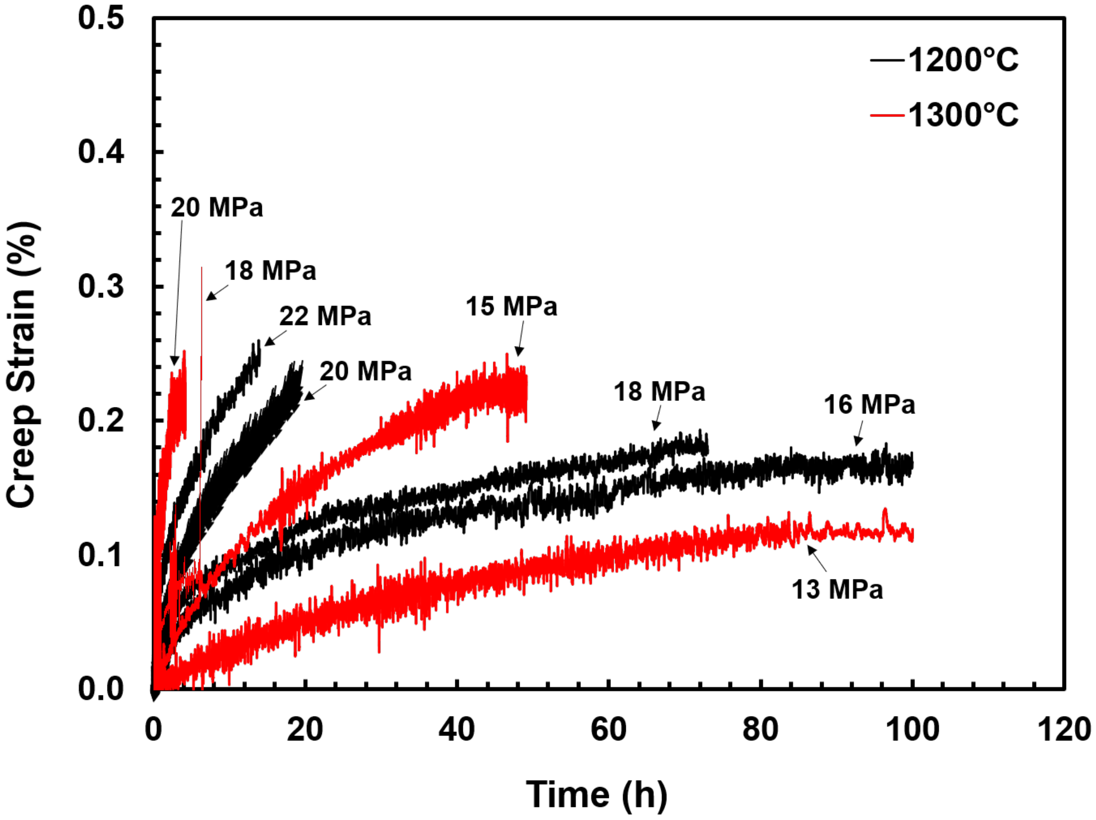

Figure 28. Creep strain vs. time curves for Hi-Nicalon$^{\text{TM}}$ SiC-B$_4$C CMC obtained at 1200°C and 1300°C in steam. Data at 1200°C from Pope[19]

Minimum creep strain rate as a function of applied interlaminar shear stress is presented in Figure 29, where results at 1200°C from prior work [19] are included for comparison. At 1300°C in air and in steam, the minimum creep rate increases by at least an order of magnitude when the applied stress increases from 13 to 20 MPa. Steam has little effect on secondary creep rates. The secondary creep rates produced in steam can be slightly higher or slightly lower than those produced in air.

However, the difference between the rates obtained in air and in steam can be viewed as simple data scatter. In contrast, an increase in temperature from 1200°C to 1300°C has a dramatic effect on minimum creep rates. For both air and steam environments, minimum creep rates produced at 1300°C can be 100 times the rates produced at 1200°C.

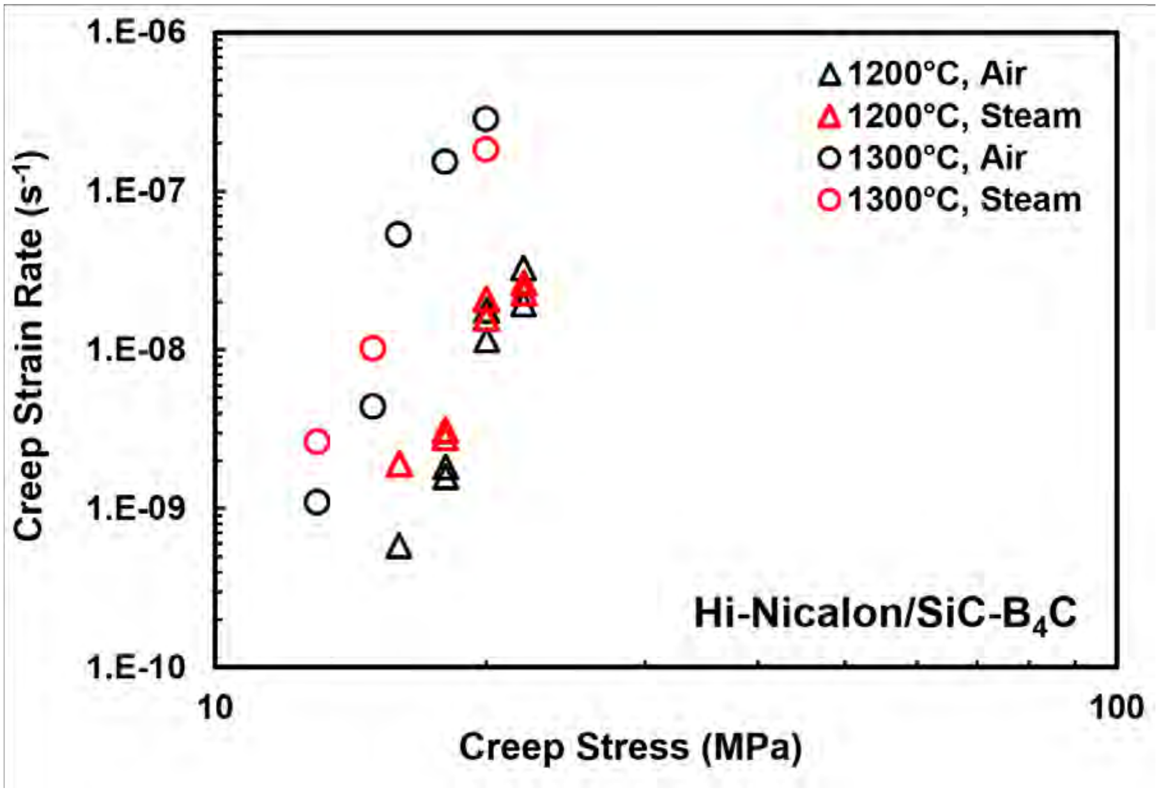

Figure 29. Minimum creep rate vs. applied interlaminar shear stress for Hi-Nicalon^{TM} SiC-B_4C CMC at 1200°C and 1300°C in air and in steam. Data at 1200°C from Pope[19]

Stress-rupture results obtained at 1300°C are summarized in Figure 30, where the results at 1200°C from prior work [19] are included for comparison. The applied shear stress vs. time to rupture data in Figure 30 demonstrate that steam has little influence on creep lifetimes. At 1300°C, creep run-out was achieved at 13 MPa in both air and steam. In fact, at higher creep stress levels, steam appears to be slightly beneficial. Note that a similar observation can be made regarding the stress-rupture results obtained in air and in steam at 1200°C. Results in Figure 30 demonstrate that increase in temperature from 1200°C to 1300°C significantly degrades creep resistance in both air and steam environments. Creep lifetimes at 1300°C can be an order of magnitude lower than those at 1200°C.

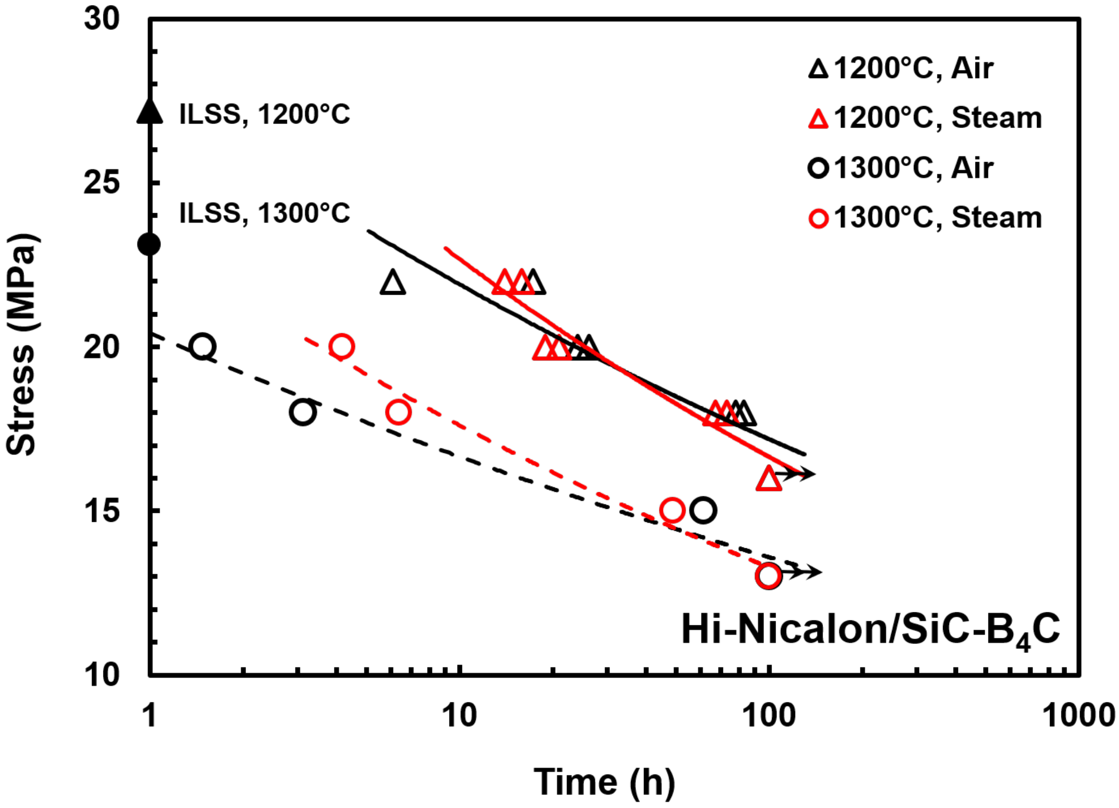

Figure 30. Interlaminar shear stress vs. time to rupture for Hi-Nicalon^{TM} SiC-B_4C CMC obtained at 1200°C and 1300°C in air and in steam. Data at 1200°C from Pope[19]

The specimens that achieved creep run-out were subsequently tested in compression to failure at 1300°C in air to evaluated retained properties. Creep at 13 MPa in air had virtually no effect on ILSS. In contrast, creep at 13 MPa in steam degraded the ILSS by nearly 10%.

5.5 Composite Microstructure

The HTPMC test specimens were examined using an optical microscope to determine the failure mode. The HTPMC specimens with and without stainless steel foil were examined. The fracture surfaces of all Hi-Nicalon^{TM} SiC-B_4C CMC test specimens were examined with an optical microscope and a SEM to gain insight into damage development and the failure mode. The bottom half of the each test specimen was used for microstructure examination. When a specimen failed, a failure detector included in the test procedure, shut down the system immediately and the bottom half of the specimen was removed from the furnace chamber. Thus, the fracture surfaces examined in this work were exposed to elevated temperature and extended oxidation only for a few minutes.

5.5.1 HTPMC Failure Examination with Optical Microscopy.

It is worth noting that one hybrid HTPMC specimen containing stainless steel foil failed by delamination prior to testing. This specimen was stored in the same location and handled in the same manner as all other specimens. The optical micrograph (Figure 31) reveals that this specimen failed in interlaminar shear due to weak adhesion between HTPMC plies and the stainless steel foil. We attribute this failure to poor performance of FM57 adhesive.

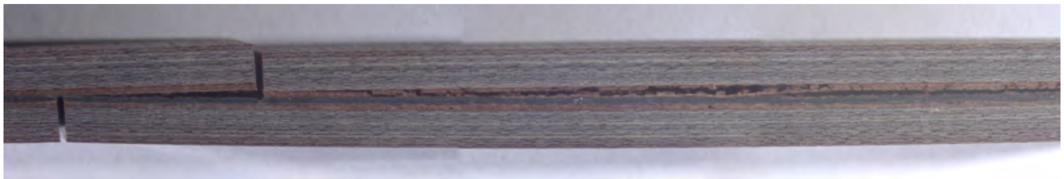

Figure 31. Hybrid HTPMC Failure Prior to Testing

Further evidence of the poor adhesive strength of the FM57 adhesive was found during testing. Figures 32 and 33 show typical failure of the non-hybrid HTPMC specimens (i.e. HTPMC specimens fabricated without stainless steel foil) tested in compression to failure. As illustrated in Figures 32 and 33, the non-hybrid HTPMC specimens fail in compression across multiple plies of the composite. There is no evidence of delamination.

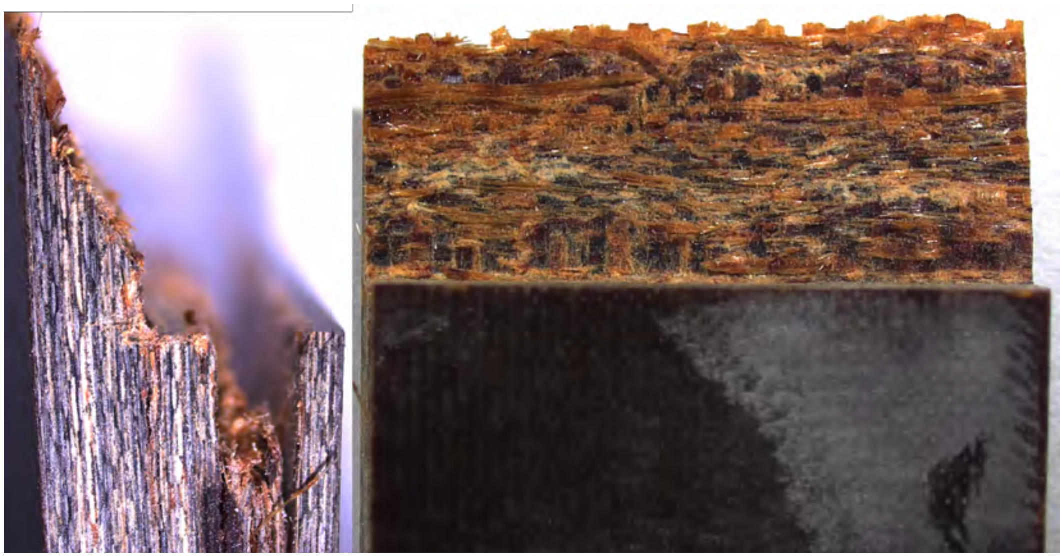

Figure 32. Non-Hybrid HTPMC - DNS specimen tested in compression to failure at 204°C

Figure 33. Non-Hybrid HTPMC - DNS specimen tested in compression to failure at 204°C

Figures 34 and 35 show typical failure of the hybrid HTPMC specimens containing stainless steel foil tested in compression to failure. All hybrid HTPMC specimens failed by interlaminar shear along the layer of FM57 adhesive. Figures 34 and 35 show clean separation of the HTPMC from the stainless steel foil. We attribute these failures to poor performance of the FM57 adhesive.

Figure 34. Hybrid HTPMC - DNS specimen tested in compression to failure at 204°C

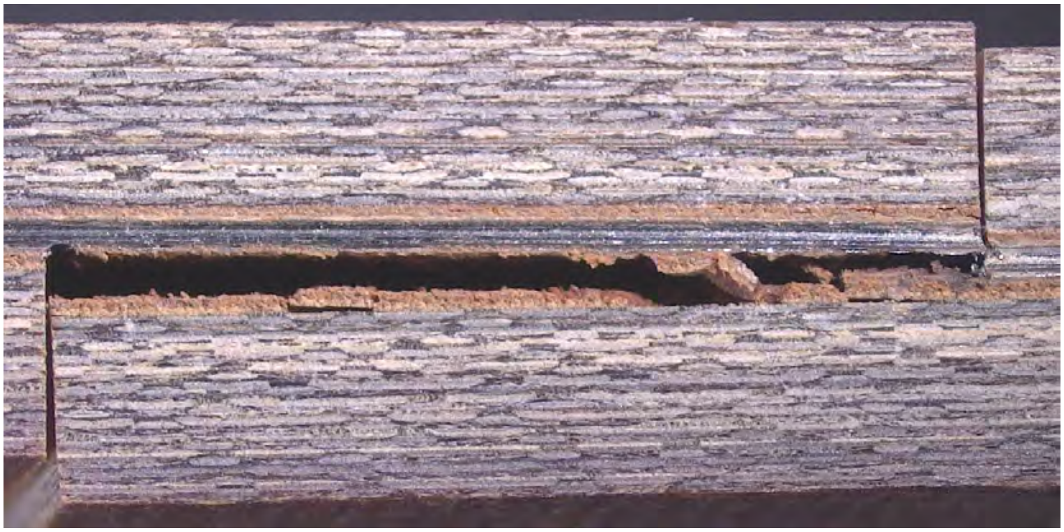

Figure 35. Hybrid HTPMC - DNS specimen tested in compression to failure at 204°C

5.5.2 CMC Microstructure.

Figure 36 shows a typical fracture surface of the DNS specimen tested in compression to failure at 1300°C in air (test duration < 5 s). Fracture occurs along the shear plane primarily through delamination of woven 0/90 fiber layers from the matrix-rich regions, with minimal fiber fracture. The fracture surface in Figure 36 is predominantly clean and smooth, indicating that a single fiber layer is associated with delamination. The fracture surface in Figure 36 indicates that a dominant failure mechanism in compression to failure test is interply delamination.

Figure 36. Fracture surface of the DNS specimen tested in compression to failure at 1300°C in air. Test duration < 5 s

Examination of the fracture surfaces produced in creep at 1300°C in air reveals that test duration has a strong influence on the failure mechanism. As the test duration increases, the failure mechanism changes from interply delamination to fracture of fiber tows. Consider a typical fracture surface produced in a creep test of shorter duration (Figure 37). The fracture surface in Figure 37 obtained in creep at 18 MPa in air (test duration = 3.13 h) is dominated by areas of clean ply delamination, whereas, fiber fracture and matrix damage are minimal.

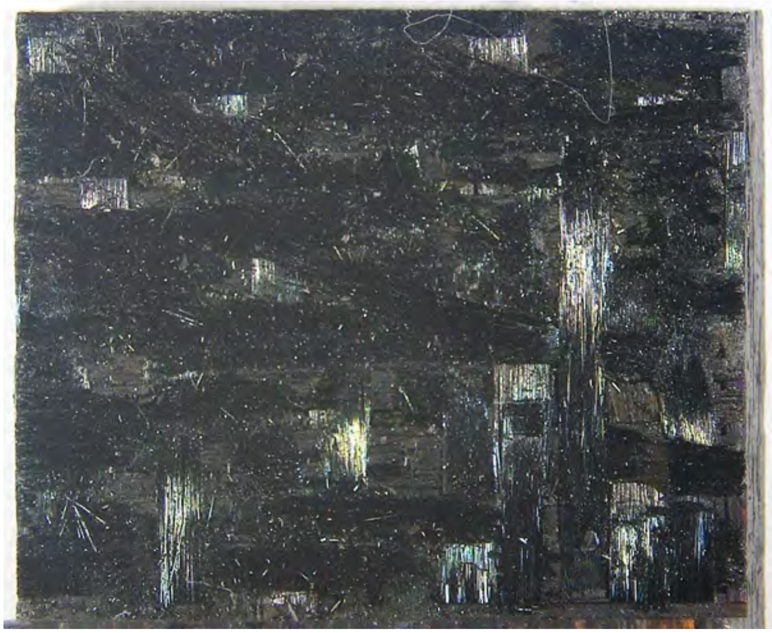

Figure 37. Fracture surface of the DNS specimen tested in creep at 18 MPa at 1300°C in air, t_f = 3.13 h

A typical fracture surface produced in a test of longer duration is shown in Figure 38. The fracture surface in Figure 38 produced in creep at 12 MPa in air (test duration > 20 h) exhibits both fiber fracture and matrix damage. Virtually no areas of clean interply delamination remain. For this longer duration creep test, the dominant failure mechanism is fracture of fiber tows.

Figure 38. Fracture surface of the DNS specimen tested in creep at 12 MPa at 1300°C in air, $t_f < 20$ h

In contrast, all fracture surfaces produced in creep tests performed at 1300°C in steam exhibit considerable areas of fiber fracture and matrix damage. Consider the fracture surface in Figure 39 produced in creep at 18 MPa in steam (test duration = 6.1 h). Despite the relatively short test duration, the fracture surface in Figure 39 displays noticeable areas of fiber fracture and matrix damage.

Figure 39. Fracture surface of the DNS specimen tested in creep at 18 MPa at 1300°C in steam, t_f = 6.1 h

Higher magnification images obtained with an SEM support these observations. Typical fracture surfaces produced in tests of shorter duration (test duration < 20 h) in air are dominated by areas of clean ply delamination (Figure 40a), only small amounts of matrix material remain bonded to the exposed fibers (Figure 40b). Small amounts of glassy phase (believed to be boria) are also observed at the periphery of the fracture surface (bubble like features in Figure 40a).

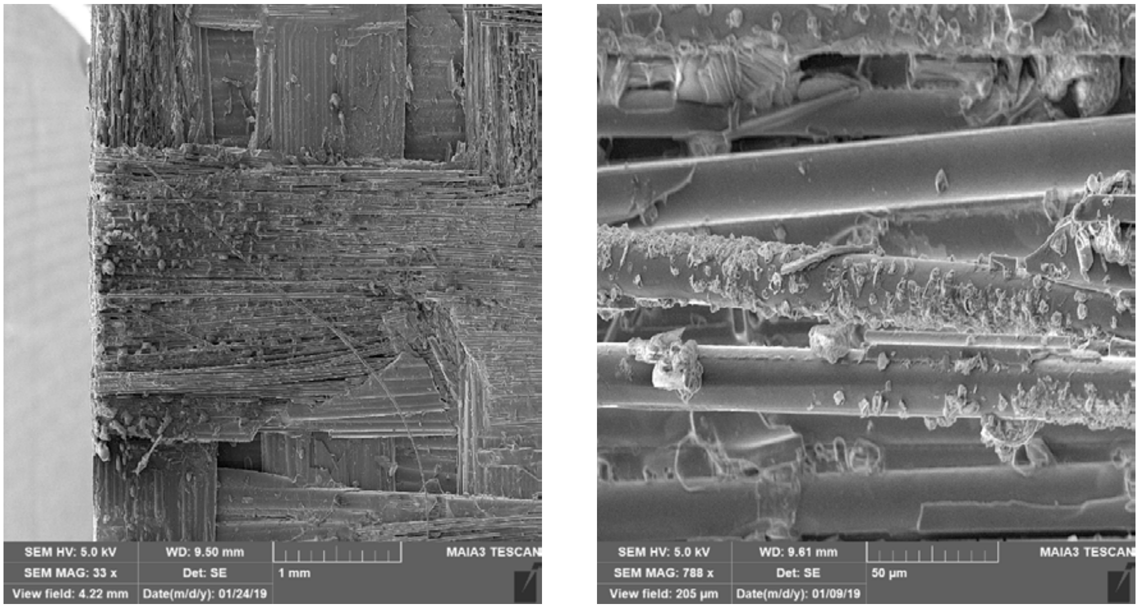

(a) (b)

Figure 40. Typical fracture surface produced in a creep test of short duration ($t_f < 20$ h) at 1300°C in air. (a) Area of clean interply delamination. (b) Small amounts of matrix material remain bonded to the exposed fibers

Conversely, typical fracture surfaces produced in tests of longer duration (test duration > 20 h) exhibit extensive fiber fracture. These fracture surface are dominated by areas of violent failure involving multiple fiber layers (Figure 41a) and widespread fiber fracture (Figure 41b). Considerable fiber-matrix bonding is also observed (Figure 41c and Figure 41d). The image shown in Figure 41c was captured near the center of the fracture surface. Note the glassy layer covering both the fibers in the background and the fracture fibers in the foreground.

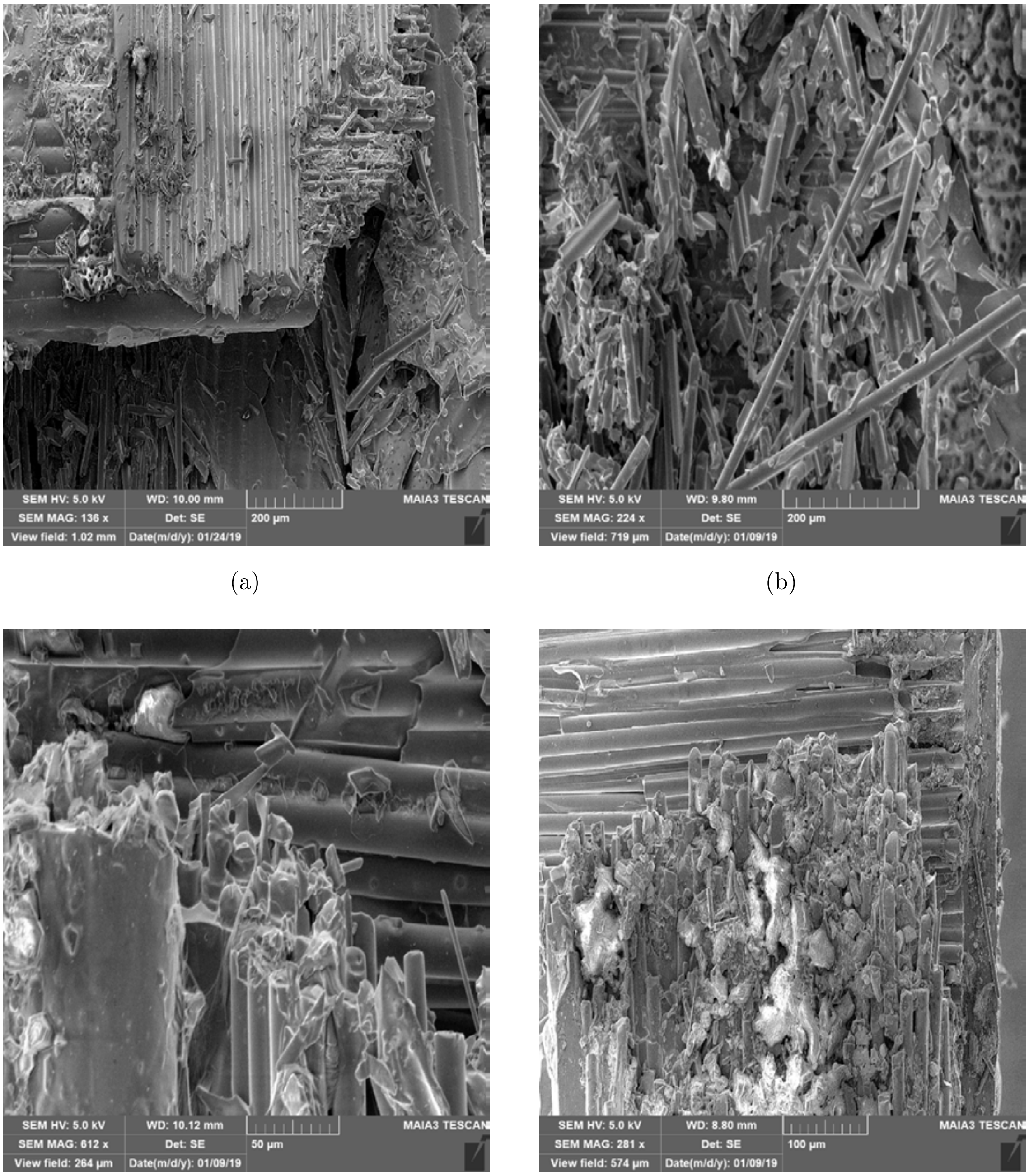

(a) (b)

(c) (d)

Figure 41. Typical fracture surface produced in a creep test of long duration ($t_f > 20$ h) at 1300°C in air. (a) Area of violent failure involving multiple fiber layers. (b) Extensive fiber fracture. (c)-(d) Fiber-matrix bonding

Typical fracture surfaces produced in creep tests performed at 1300°C in steam exhibit considerable areas of fiber fracture and matrix damage. Key features of a typical fracture surface produced in creep in steam are: areas of violent failure involving multiple fiber layers noticeable (Figure 42a), fiber-matrix bonding (Figure 42b), and extensive fiber fracture (Figure 42c and Figure 42d).

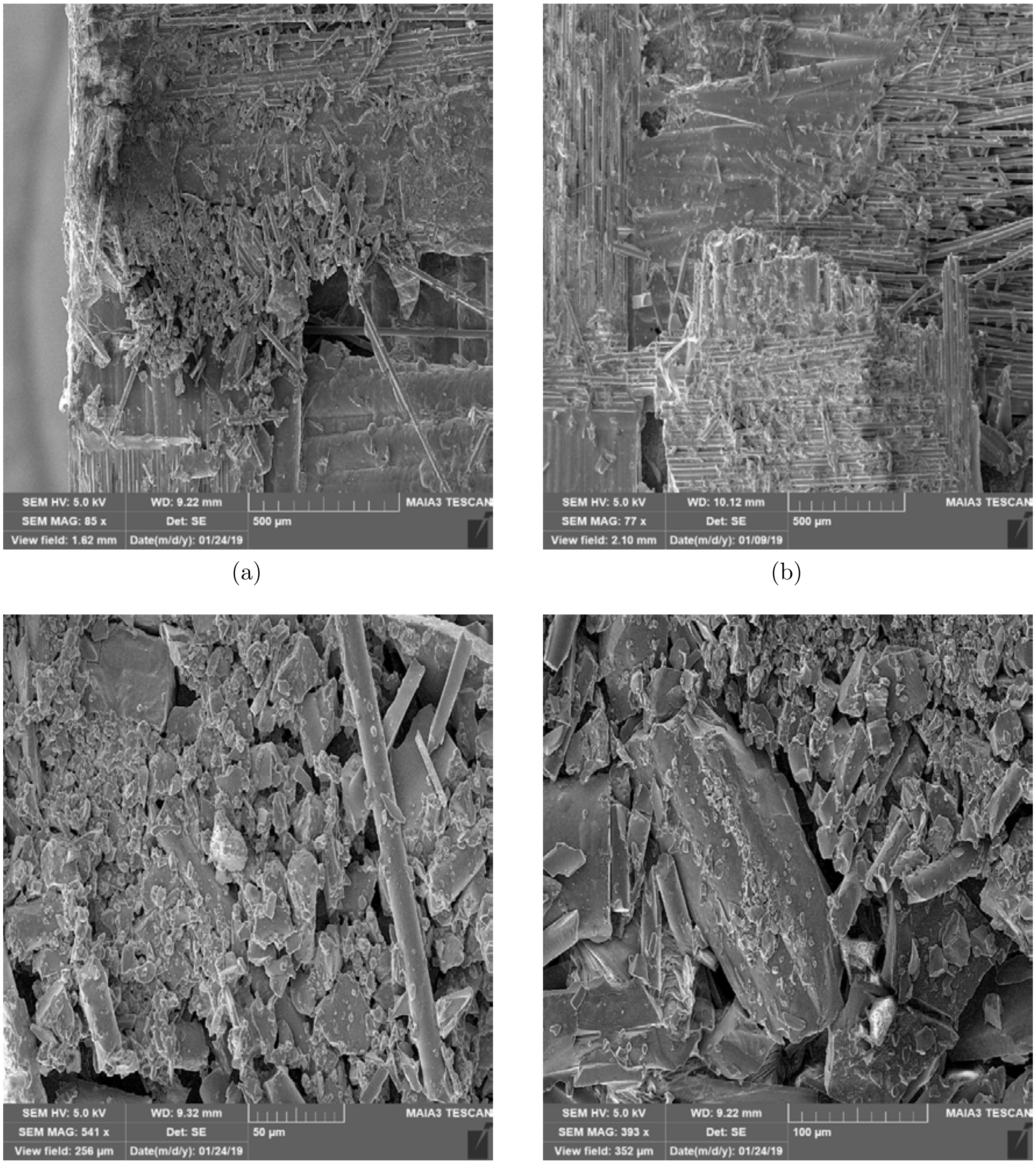

(a) (b)

(c) (d)

Figure 42. Typical fracture surface produced in creep test at 1300°C in steam. (a) Area of violent failure involving multiple fiber layers. (b) Fiber-matrix bonding. (c)-(d) Extensive fiber fracture

The fracture surfaces produced in creep in interlaminar shear at 1200°C in air showed minimal amounts of glassy phase at the edges and virtually none in the interior[19]. However, a much greater amount of the glassy phase was observed on fracture surfaces produced at 1200°C in steam[19]. In contrast, the SEM examination of the fracture surfaces produced in creep tests at 1300°C in air and in steam reveals significant formation of the glassy phase. The glassy phase covers the periphery of the fracture surfaces as well as large portions of the interior. Typical fracture surfaces obtained at 1300°C in steam exhibit even larger amounts of glassy phase, in many cases, covering nearly half of the fracture surface. Higher magnification images show formation of the glassy phase at the edge of the fracture surface (Figure 43a and Figure 43b). The image in Figure 43b shows that glassy phase formed at the edge of the fracture surface has crystallized and cracks have developed after cooling down to room temperature.

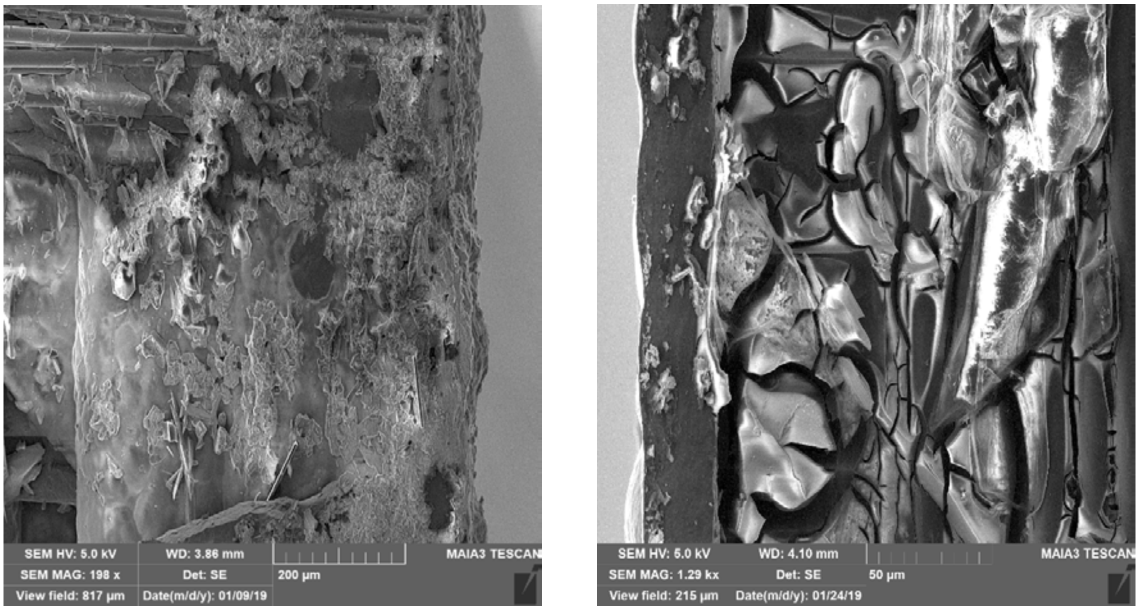

(a) (b)

Figure 43. Typical fracture surface produced in a creep test of short duration ($t_f < 20$ h) at 1300°C. (a) Glassy phase at the periphery of the fracture surface. (b) Cracks in the crystallized glassy phase at the edge of the fracture surface

Figure 44 shows evidence of a glassy phase covering oxidized regions of a typical fracture surface.

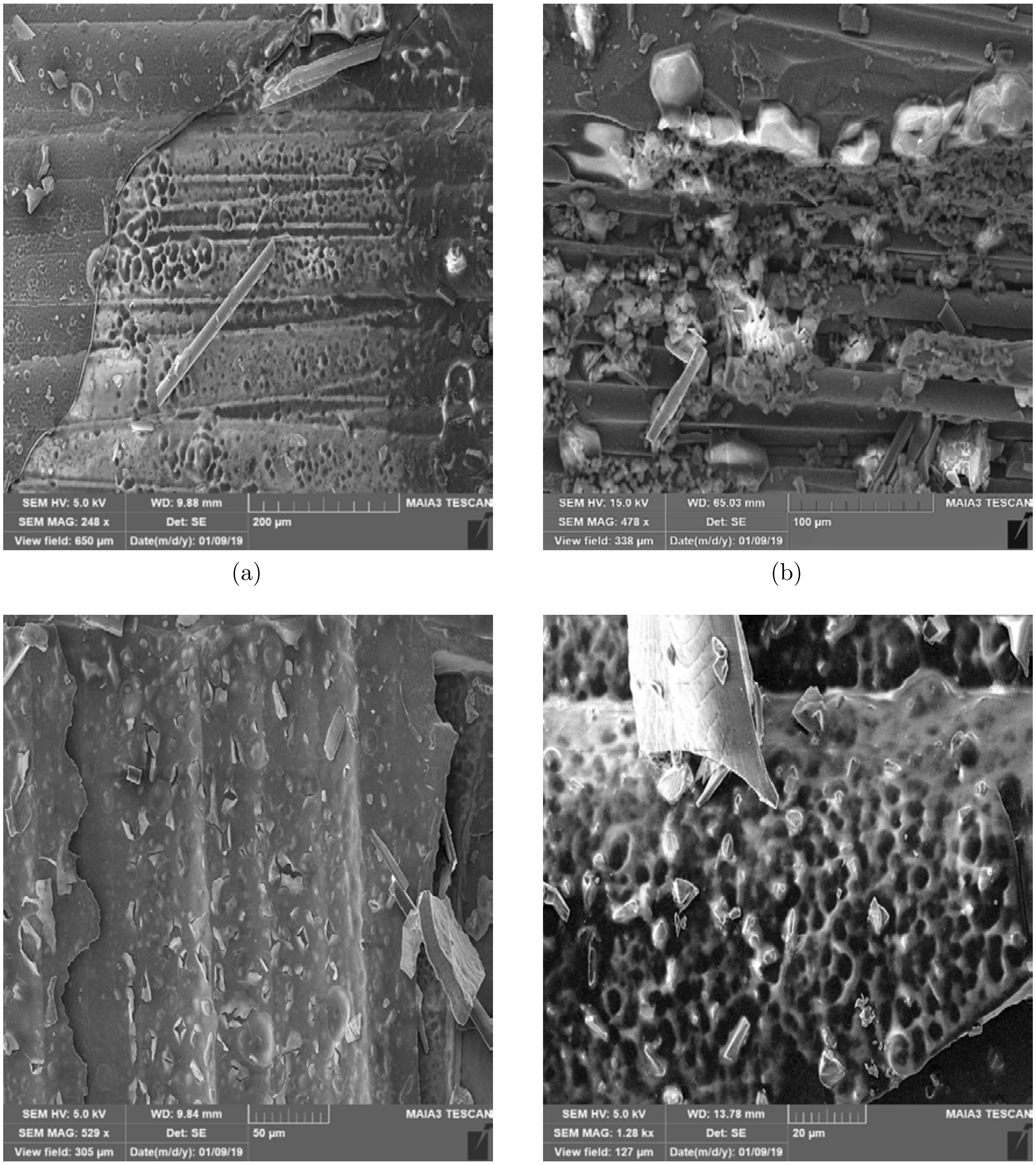

(a) (b)

(c) (d)

Figure 44. Typical fracture surface produced in creep test at 1300°C. Glassy phase covering portions of the fracture surface interior

Recall that the Hi-Nicalon^{TM} SiC-B_4C CMC has an oxidation-inhibiting matrix consisting of concentric layers of SiC and the crack arresting B_4C around groups of fibers. At 1300°C, in both air and steam environments, SiC and B_4C react with oxygen that enters through matrix cracks. As a result, fluid glassy phases are produced that fill the matrix cracks as soon as they are initiated, thereby impeding the diffusion of oxygen through those cracks. This is what give the composite improved oxidation resistance. Matrix cracks are initiated when the compressive load is applied. Because the DNS specimens are loaded in compression, glassy phases formed within the matrix cracks are forced out of the cracks towards the specimen edges. Apparently, the amount of glassy phase produced in tests at 1300°C is large enough to cover a sizable portion of the interior of the fracture surface in addition to covering its periphery. Additionally, the increased regions of glassy phase observed in the presence of steam is attributed to the increased oxidation rate due to the presence of steam. It has been reported that parabolic oxidation rate of SiC has proportional relationship to the partial pressure of water vapor[27]. The increased creep strains observed in steam testing are attributed to this increased rate of oxidation.

Furthermore, at 1300°C in air as well as in steam, the oxidation of the B_4C layers and formation of boria glass is likely followed by the oxidation of the SiC matrix layers. As a result, borosilicate glass forms during the test. Bubbles in the glassy layer covering the fracture surfaces in Figure 44a and Figure 44b are believed to be the gaseous reaction products diffusing through the borosilicate glass. Viscosity of the borosilicate glass is higher than that of boria glass. Therefore, it is more difficult for the gaseous reaction products to escape through the borosilicate glass layer[28].

VI. Conclusions and Recommendations

Interlaminar shear properties of an AFR-PE-4/ Astroquartz-III HTPMC and a Hi-Nicalon^{TM} SiC-B$_4$C CMC were evaluated at elevated temperature. Two variants of the HTPMC were considered: (1) a HTPMC and (2) a HTPMC with stainless steel foil at the midplane. Double notch shear (DNS) specimens were used in all tests. Interlaminar shear strength (ILSS) of all materials was measured in compression tests to failure. All HTPMC specimens were tested at 204°C in laboratory air. The CMC specimens were tested at 1300°C in air and in steam.

Addition of the stainless steel foil to the HTPMC resulted in significant loss of ILSS. The ILSS of the HTPMC specimens containing stainless steel foil was on average 58% lower than the ILSS of the HTPMC specimens fabricated without foil. All HTPMC specimens containing stainless steel foil failed by delamination due to weak bonding between the stainless steel foil and the HTPMC. Because the HTPMC variant with the stainless steel foil studied in this work produced poor interlaminar shear properties, we do not recommend any further investigation of this HTPMC variant. We recommend that different adhesives and/or alternate methods of fabricating HTPMC specimens with the stainless steel foil be explored.

Creep behavior in interlaminar shear of the Hi-Nicalon^{TM} SiC-B$_4$C CMC was studied at 1300°C in laboratory air and in steam. The DNS specimens were used in all tests. The average ILSS was 23 MPa. Creep-rupture tests at 1300°C in air and steam were performed at stress levels ranging from 13 MPa (57% ILSS) to 20 MPa (87% ILSS). Primary and secondary creep regimes were observed in all tests. Tertiary creep was not observed. Creep run-out of 100 h was achieved at 13 MPa in both air and steam environments. Creep strains produced at 13 MPa in air are similar to the failure strains produced in compression to failure tests. Creep strains produced at stresses $\geq$ 15 MPa significantly exceed the strains produced in compression tests.

While steam has virtually no effect on the creep run-out stress, it has considerable effect on creep strains. Significantly larger creep strains are accumulated in steam than in air. At 1300°C steam has negligible effect on minimum creep strain rates. At 1300°C minimum creep strain rates range from 1.08 x 10^{-9} s^{-1} to 2.8 x 10^{-7} s^{-1} in air and from 2.6 x 10^{-9} s^{-1} to 1.8 x 10^{-7} s^{-1} in steam. At 1300°C steam has little influence on creep lifetimes. The presence of steam appears to be slightly beneficial at higher creep stress levels. Prior creep at 1300°C in air had little effect on ILSS. Conversely, prior creep in steam reduced the ILSS by nearly 10%.

Comparison with data at 1200C from prior effort [19] revealed that increase in temperature from 1200°C to 1300°C resulted in approximately 15% loss in ILSS. An increase in temperature from 1200°C to 1300°C significantly degrades creep performance of this CMC in air as well as in steam. Larger creep strains are accumulated at 1300°C than at 1200°C. Moreover, much shorter creep lifetimes are produced at 1300°C than at 1200°C in both air and steam environments. An increase in temperature from 1200°C to 1300°C also has a dramatic effect on minimum creep rates. For both air and steam environments, minimum creep rates produced at 1300°C can be 100 times the rates produced at 1200°C. Finally, an increase in temperature from 1200°C to 1300°C significantly degrades creep resistance in both air and steam environments. Creep lifetimes at 1300°C can be an order of magnitude lower than those at 1200°C. At 1300°C in air and in steam environments, the prevailing failure mechanism changes with increasing test duration. Interply delamination is the dominant failure mechanism in tests of short duration. In contrast, in tests of longer duration (test duration $>$ 20 h) multiple woven fiber layers are associated with failure, fiber fracture becomes the dominant failure mechanism.

Results of this work are promising. We recommend that mechanical behavior of this CMC at 1300°C be explored further. We also recommend that an additional systematic study of failure mechanisms in interlaminar shear be performed at 1300°C. More testing at 1300°C in air and especially in steam is recommended. Only a limited number of test specimens was available for this study. A follow-on study involving multiple tests per condition would be beneficial. Additionally, elemental analysis of the glassy phases noted in the fracture surface is recommended.

Appendix A. Additional HTPMC Micrographs

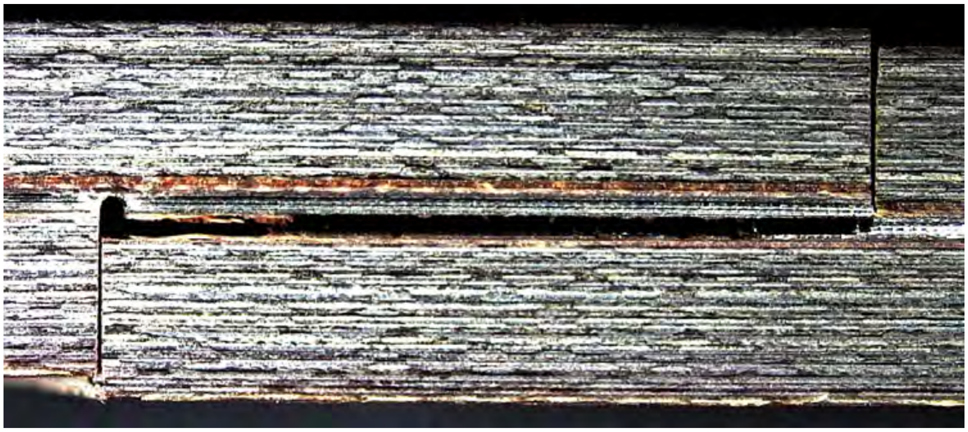

Figure 45. Hybrid HTPMC - DNS specimen tested in compression to failure at 204.4°C

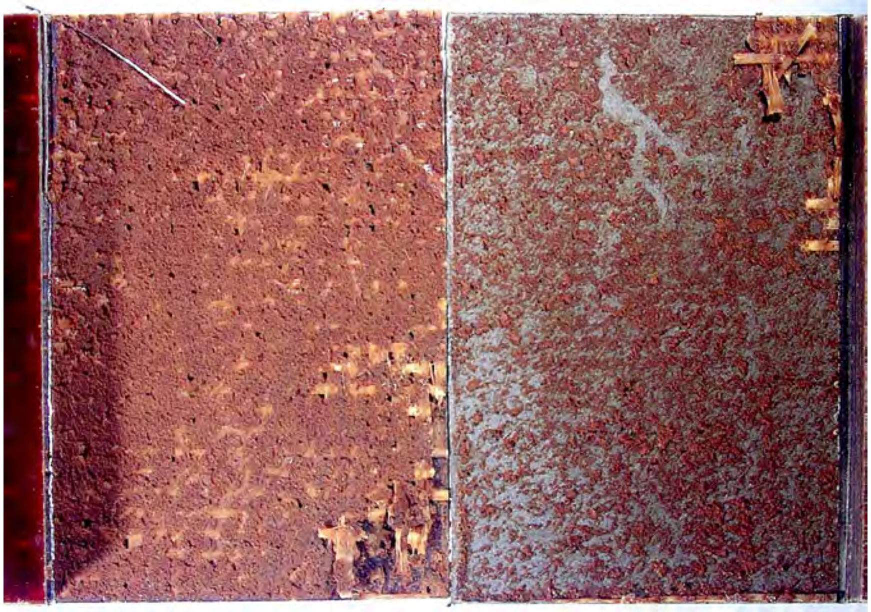

Figure 46. Hybrid HTPMC - Top and Bottom of DNS specimen tested in compression to failure at 204.4°C

Figure 47. Hybrid - Top and Bottom of DNS specimen tested in compression to failure at 204.4°C

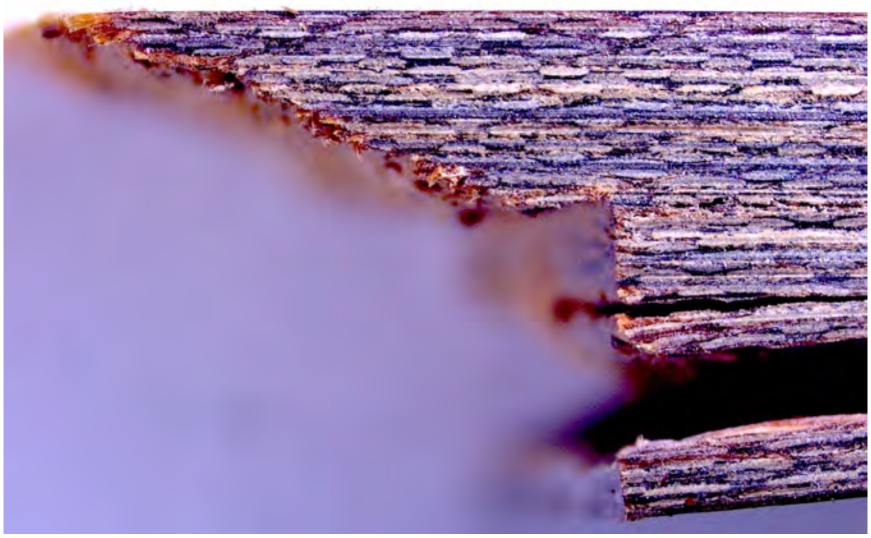

Figure 48. Non-Hybrid - Top and Bottom of DNS specimen tested in compression to failure at 204.4°C

Appendix B. Additional CMC Micrographs

Figure 49. Fracture surface of the DNS specimen tested in creep at 14 MPa at 1300°C in air

Figure 50. Fracture surface of the DNS specimen tested in creep at 16 MPa at 1300°C in air

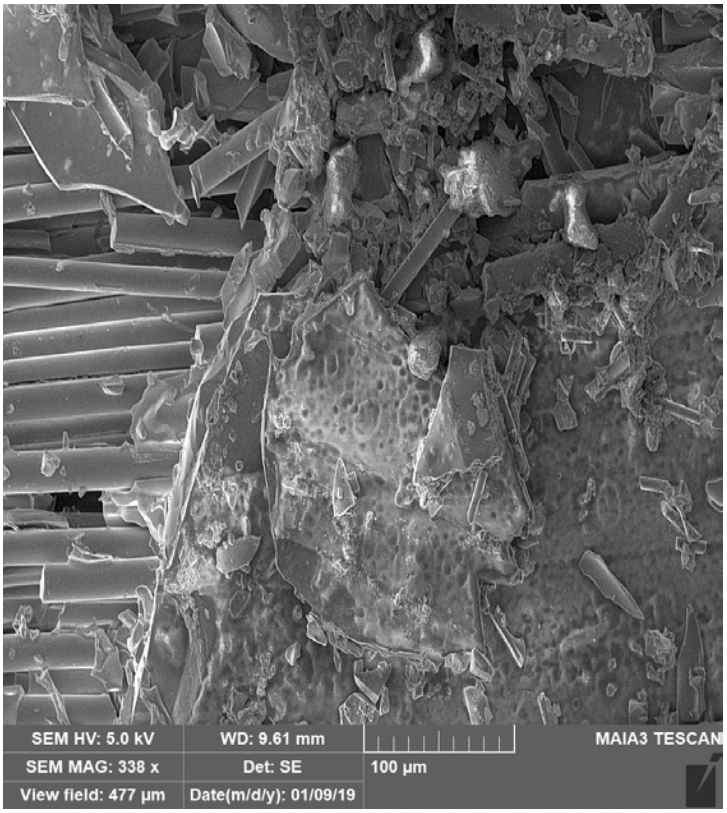

Figure 51. Fiber and Matrix Debris on the DNS specimen tested in creep at 16 MPa Creep at 1300°C in air

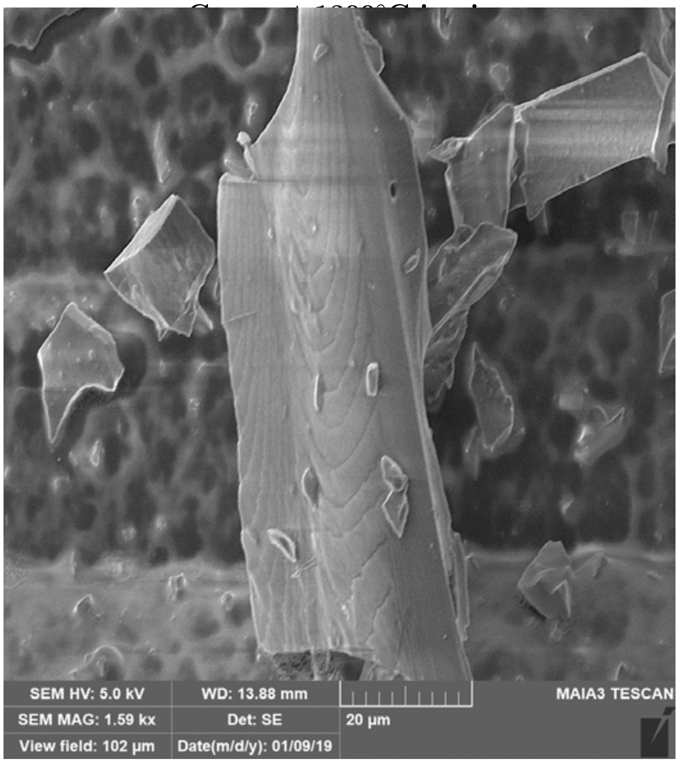

Figure 52. Matrix Debris and Borosilicate Glass on the DNS specimen tested in creep at 16 MPa Creep at 1300°C in air

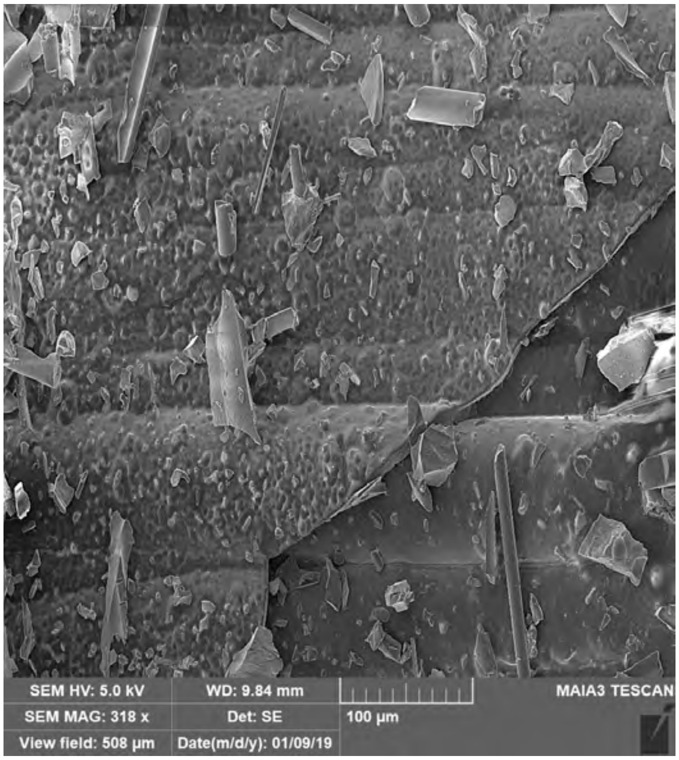

Figure 53. Glassy Phase and Matrix Debris on the DNS specimen tested in creep at 16 MPa Creep at 1300°C in air

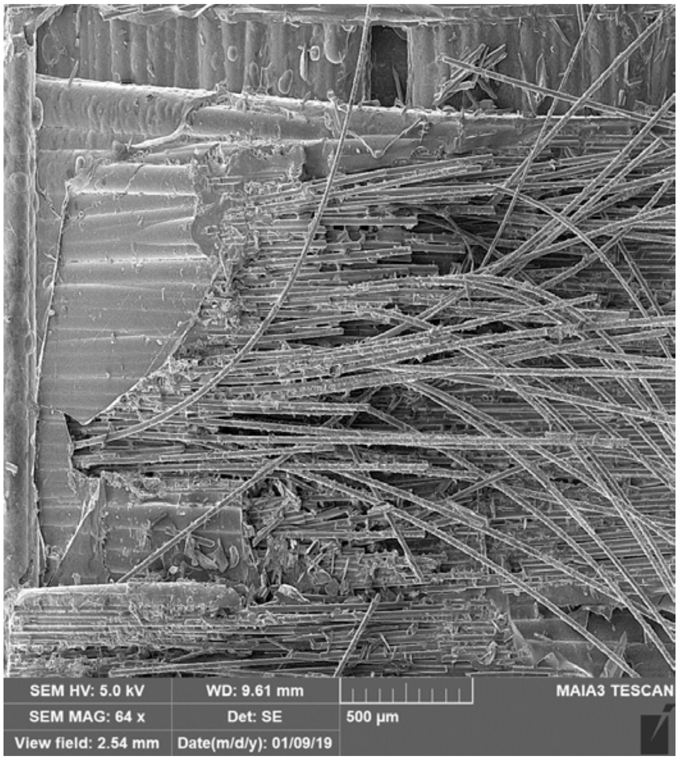

Figure 54. Fiber Fracture on the DNS specimen tested in creep at 16 MPa Creep at 1300°C in air

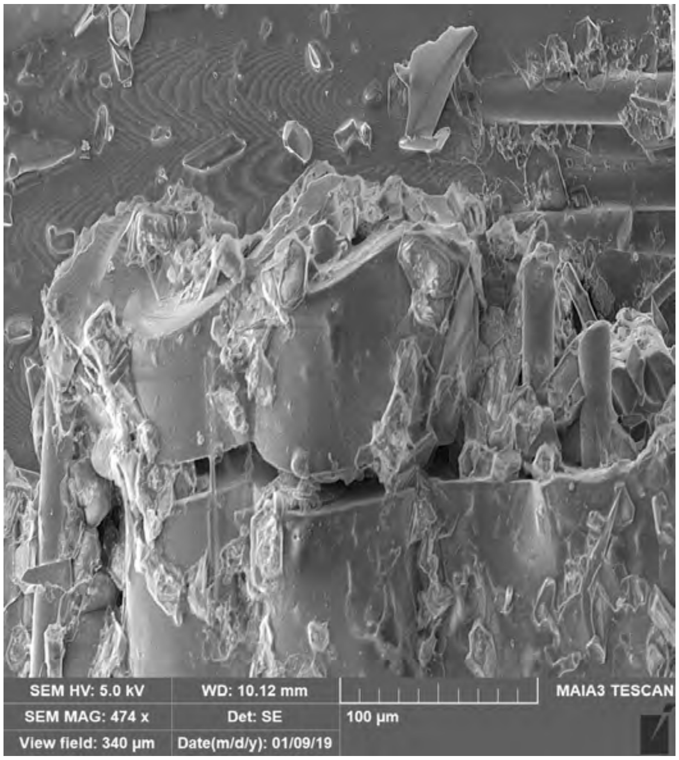

Figure 55. Broken Fibers and Matrix on the DNS specimen tested in creep at 12 MPa Creep at 1300°C in air

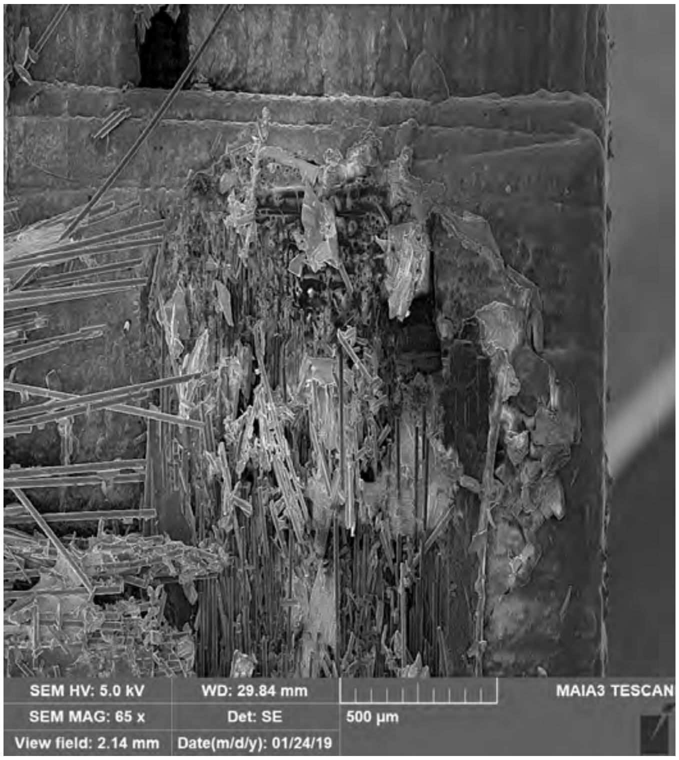

Figure 56. Glassy Phase at the periphery on the DNS specimen tested in creep at 12 MPa Creep at 1300°C in air

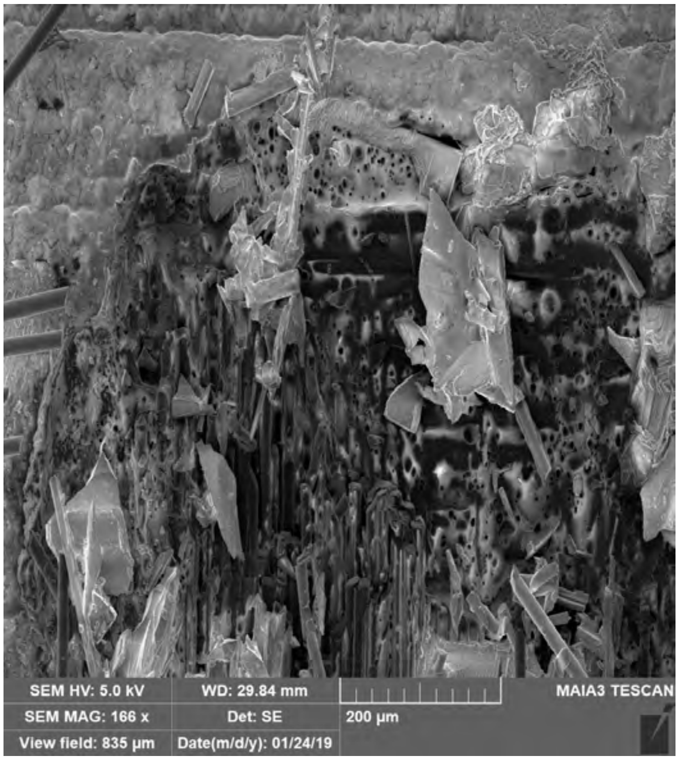

Figure 57. Borosillicate Glass at the periphery on the DNS specimen tested in creep at 12 MPa Creep at 1300°C in air

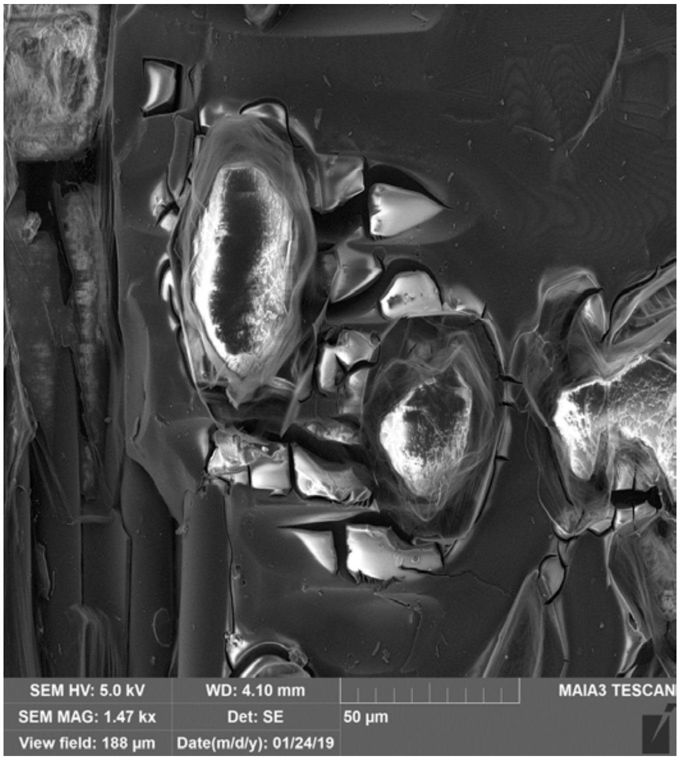

Figure 58. Glass formation on the DNS specimen tested in creep at 18 MPa Creep at 1300°C in air

Bibliography

1. K. K. Chawla, *Composite Materials.* New York, NY: Springer New York, 3rd ed., 2012.
2. T. Becher, A. Broggio, and A. Ferroglia, "Composite Materials," in *Mechanical Engineers' Handbook, Volume 1: Materials and Engineering Mechanics* (M. Kutz, ed.), ch. 10, Hoboken, NJ, USA: John Wiley & Sons, Inc., 4th ed., 12 2015.
3. D. D. Chung, *Composite Materials.* Engineering Materials and Processes, London: Springer London, 2010.
4. R.-M. Wang, S.-R. Zheng, and Y.-P. G. Zheng, *Polymer Matrix Composites and Technology.* Cambridge, UK: Woodhead Publishing Limited, 2011.
5. P. Mallick, *Fiber-Reinforced Composites.* No. 3 in Dekker Mechanical Engineering, Boca Raton, FL: CRC Press, 11 2007.
6. R. M. Koide, G. Z. D. Franca, and M. A. Luersen, "An Ant Colony Algorithm Applied to Lay-up Optimization of Laminated Composite Plates," *Latin American Journal of Solids and Structures*, vol. 10, pp. 491–504, 2013.
7. M. Davies, "Properties of Materials and Structural Considerations," in *Standard Handbook for Aeronautical and Astronautical Engineers.*, pp. 11–35, McGraw-Hill Professional, 2003.
8. A. Baker, S. Dutton, and K. Kelly, *Composite Materials for Aircraft Structures. AIAA Education Series.* American Institute of Aeronautics and Astronautics, Inc., 2011.
9. C. R. Schultheisz and A. M. Waas, "Compressive failure of composites, Part I: Testing and micromechanical theories," *Progress in Aerospace Sciences*, vol. 32, no. 1, pp. 1–42, 1996.
10. S. Sridharan, *Delamination Behaviour of Composites.* Cambridge, UK: Woodhead Publishing Limited, 2008.
11. S. Schmidt, S. Beyer, H. Knabe, H. Immich, R. Meistring, and A. Gessler, "Advanced ceramic matrix composite materials for current and future propulsion technology applications," *Acta Astronautica*, vol. 55, no. 3-9, pp. 409–420, 2004.
12. K. K. Chawla, *Ceramic Matrix Composites.* London, England: Chapman & Hall, 1st ed., 1993.
13. M. P. Wilkinson, *Mechanical Properties And Fatigue Behavior Of Unitized Composite Airframe Structures At Elevated Temperature.* PhD thesis, Air Force Institute of Technology, 2014.

14. T. Beumler, *Flying GLARE - A contribution to aircraft certification issues on strength properties in non-damaged and fatigue damaged GLARE structures.* MG Delft, Netherlands: Delft University Press Science, 2004.

15. W. Callister, *Materials Science and Engineering: an Introduction.* John Wiley & Sons, Inc, 8th ed., 2 2010.

16. C. A. Harper, "Handbook of Plastics, Elastomers, and Composites," in *Handbook of Plastics, Elastomers, and Composites*, New York: McGraw-Hill Professional, 4th ed., 2002.

17. J. F. Laliberte, C. Poon, P. V. Straznicky, and A. Fahr, "Applications of Fiber-Metal Laminates," *Polymer Composites*, vol. 21, no. 4, pp. 558–567, 2000.

18. R. C. Alderliesten and J. J. Homan, "Fatigue and damage tolerance issues of Glare in aircraft structures," *International Journal of Fatigue*, vol. 28, pp. 1116–1123, 2006.

19. M. T. Pope, *Creep Behavior In Interlaminar Shear Of A CVI SiC/SiC Composite At Elevated Temperature In Air And In Steam.* PhD thesis, Air Force Institute of Technology, 2012.

20. S. R. Choi, R. W. Kowalik, D. J. Alexander, and N. P. Bansal, "Elevated-temperature stress rupture in interlaminar shear of a Hi-Nic SiC/SiC ceramic matrix composite," *Composites Science and Technology*, vol. 69, no. 7-8, pp. 890–897, 2009.

21. J. Singh, N. P. Bansal, and W. M. Kriven, *Advances in Ceramic Matrix Composites.* Westerville, Ohio: The American Ceramic Society, 2005.

22. ASTM, "C1425 - Standard Test Method Interlaminar Shear Strength of 1D and 2D Continuous Fiber-Reinforced Advanced Ceramics at Elevated Temperatures," tech. rep., ASTM International, West Conshohocken, PA, 2013.

23. N. J. Fang and T.-W. Chou, "Characterization of Interlaminar Shear Strength of Ceramic Matrix Composites," *Journal of the American Ceramic Society*, vol. 76, no. 10, pp. 2539–2548, 1993.

24. K. T. Kedward, "On the short beam test method," *Fibre Science and Technology*, vol. 5, no. 2, pp. 85–95, 1972.

25. K. Whitley and T. Collins, "Mechanical Properties of T650-35/AFRPE-4 at Elevated Temperatures for Lightweight Aeroshell Designs," tech. rep., NASA Langley Research Center, Hampton, VA, 2012.

26. S. Zhu, M. Mizuno, Y. Nagano, J. Cao, Y. Kagawa, and H. Kaya, "Creep and Fatigue Behavior in an Enhanced SiC / SiC Composite at," *Journal of the American Ceramic Society*, vol. 77, pp. 2269–2277, 1998.

27. E. J. Opila and R. E. Hann, “Paralinear oxidation of CVD SiC in water vapor,” *Journal of the American Ceramic Society*, vol. 80, no. 1, pp. 197–205, 1997.

28. M. Lee, *Fatigue Behavior of an Advanced SiC/SiC Composite at 1300° C in Air and Steam.* PhD thesis, Air Force Institute of Technology, 2016.

REPORT DOCUMENTATION PAGE

Form Approved
OMB No. 0704–0188

The public reporting burden for this collection of information is estimated to average 1 hour per response, including the time for reviewing instructions, searching existing data sources, gathering and maintaining the data needed, and completing and reviewing the collection of information. Send comments regarding this burden estimate or any other aspect of this collection of information, including suggestions for reducing this burden to Department of Defense, Washington Headquarters Services, Directorate for Information Operations and Reports (0704–0188), 1215 Jefferson Davis Highway, Suite 1204, Arlington, VA 22202–4302. Respondents should be aware that notwithstanding any other provision of law, no person shall be subject to any penalty for failing to comply with a collection of information if it does not display a currently valid OMB control number. **PLEASE DO NOT RETURN YOUR FORM TO THE ABOVE ADDRESS.**

1. REPORT DATE *(DD–MM–YYYY)*
21–03–2019

2. REPORT TYPE
Master's Thesis

3. DATES COVERED *(From — To)*
Sept 2017 — Mar 2019

4. TITLE AND SUBTITLE
Interlaminar Shear Performance of High Temperature Composites

5a. CONTRACT NUMBER

5b. GRANT NUMBER

5c. PROGRAM ELEMENT NUMBER

6. AUTHOR(S)
Wallis, Tyler A., Capt

5d. PROJECT NUMBER

5e. TASK NUMBER

5f. WORK UNIT NUMBER

7. PERFORMING ORGANIZATION NAME(S) AND ADDRESS(ES)
Air Force Institute of Technology
Graduate School of Engineering and Management (AFIT/EN)
2950 Hobson Way
WPAFB OH 45433-7765

8. PERFORMING ORGANIZATION REPORT NUMBER
AFIT-ENY-MS-19-M-250

9. SPONSORING / MONITORING AGENCY NAME(S) AND ADDRESS(ES)
Intentionally Left Blank

10. SPONSOR/MONITOR'S ACRONYM(S)

11. SPONSOR/MONITOR'S REPORT NUMBER(S)

12. DISTRIBUTION / AVAILABILITY STATEMENT
Distribution Statement A:
Approved for Public Release; distribution unlimited.

13. SUPPLEMENTARY NOTES
This work is declared a work of the U.S. Government and is not subject to copyright protection in the United States.

14. ABSTRACT

Interlaminar shear properties of a high temperature polymer matrix composite (HTPMC) and a ceramic matrix composite (CMC) were evaluated at elevated temperature. Two variants of the HTPMC (AFR-PE-4) were studied: one that contained stainless steel foil at the midplane and one variant did not. The interlaminar shear strength (ILSS) of both variants of the HTPMC was evaluated at 204C in laboratory air. The addition of the stainless steel foil resulted in significant loss of ILSS for the HTPMC. The CMC studied in this work was fabricated via chemical vapor infiltration. The CMC had an oxidation-inhibited matrix consisting of alternating layers of SiC and B4C and was reinforced with Hi-Nicalon fibers. Fiber preforms had pyrolytic carbon coating and boron carbide overlay. The ILSS of the CMC was measured at 1300C in laboratory air. Additionally, creep performance in interlaminar shear of the CMC was evaluated at 1300C in air and in steam. The creep behavior was assessed for interlaminar shear stresses varying from 12 MPa to 20 MPa in air and in steam. In air and in steam, creep run-out of 100 h was achieved at 13 MPa. Both primary and secondary creep regimes were noted in all tests. Presence of steam had little effect on creep performance. The retained properties of the specimens that attained run-out were characterized.

15. SUBJECT TERMS
Composite Materials, Polymer Matrix Composite, Ceramic Matrix Composite, Polyimide, AFR-PE-4, Hybrid Laminate, Ceramic Fibers, Ceramic Materials, Fiber Reinforced Composites, HyperSiC

16. SECURITY CLASSIFICATION OF: a. REPORT	b. ABSTRACT	c. THIS PAGE	17. LIMITATION OF ABSTRACT	18. NUMBER OF PAGES
U	U	U	UU	116

19a. NAME OF RESPONSIBLE PERSON
Dr. Marina Ruggles-Wrenn

19b. TELEPHONE NUMBER *(include area code)*
(937) 255-3636, x4641; marina.ruggles-wrenn@afit.edu